LBNL-47715

Asymmetries Between Strange and Antistrange Particle Production in Hadron-Proton Interactions[1]

T.D. Gutierrez[a] and R. Vogt[a,b]

[a]Physics Department
University of California at Davis
Davis, California 95616
and
[b]Nuclear Science Division
Lawrence Berkeley National Laboratory
Berkeley, California 94720

ABSTRACT

Recent measurements of the asymmetries between Feynman x distributions of strange and antistrange hadrons in $\pi^- A$ interactions show a strong effect as a function of x_F. We calculate strange hadron production in the context of the intrinsic model and make predictions for particle/antiparticle asymmetries in these interactions.

PACS numbers: 12.38.Lg, 13.85.Ni, 14.20.Jn

[1]This work was supported in part by the Director, Office of Energy Research, Division of Nuclear Physics of the Office of High Energy and Nuclear Physics of the U. S. Department of Energy under Contract Number DE-AC03-76SF00098.

1 Introduction

Flavor correlations between the final-state hadron and the projectile have been observed in charm hadroproduction. A strong leading particle effect was seen in the difference between the D^- and D^+ distributions at large Feynman x, $x_F = p_{||}/p_{\max}$, with pion projectiles [1, 2, 3, 4, 5, 6]. More recently, hyperon beams have been used to study charm baryon distributions at high x_F [7, 8, 9, 10]. Several of these experiments [7, 8, 9, 10, 11] have also studied the x_F-dependent asymmetry between charm and anticharm baryons. This asymmetry is defined as the ratio of, for example, the difference between the Λ_c and $\overline{\Lambda}_c$ x_F distributions divided by their sums. Only recently has such data become available in the strange sector [12, 13].

The strange/antistrange baryon asymmetries A_Λ, A_{Ξ^-}, and A_Ω have been measured in π^--induced interactions at 500 GeV by the E791 Collaboration [12, 13]. The measurements are around $|x_F| < 0.1$. They find that for $x_F > 0$, A_Λ and A_Ω are nearly independent of x_F while A_{Ξ^-} increases with x_F. On the other hand, at negative x_F, only A_Ω is independent of x_F. The other asymmetries increase as x_F decreases with $A_\Lambda > A_{\Xi^-}$. These measurements are inconsistent with PYTHIA [14] which produces essentially no asymmetry at forward x_F while at negative x_F, only A_Λ is increasing. The trends of the data are consistent with qualitative expectations from recombination models [12, 13].

One such model that involves recombination with valence quarks was first developed to explain large x production of charm in the proton structure function, the "intrinsic charm" model originally motivated in Refs. [15, 16]. The model, including leading-twist $c\overline{c}$ production was extended to charm hadron asymmetries such as A_{D^-} in subsequent works [17, 18, 19]. In this picture, the projectile can fluctuate into a Fock state configuration with at least one $c\overline{c}$ pair as well as other light $q\overline{q}$ pairs. These charm quarks are comoving with the other partons in the Fock state and thus can combine with these comoving partons to produce charm hadrons at large x_F. The probability that the projectile fluctuates into a state with the projectile valence quarks and a $c\overline{c}$ pair is $\approx 0.3\%$ [20]. The probability for intrinsic states with other $Q\overline{Q}$ pairs scales as the square of the constituent quark mass. Since strange quarks are lighter than charm quarks, the corresponding probability for intrinsic $s\overline{s}$ pairs in the wavefunction should be significantly larger.

In this paper, we apply the combined leading-twist/intrinsic model of Ref. [19] to strangeness production. We describe how we calculate strangeness production at leading twist in Section 2. Section 3 is devoted to a description of the intrinsic model for strange quarks. Section 4 presents the calculations of strange hadron production asymmetries in $\pi^- p$ interactions for both positive and negative x_F, the pion and proton fragmentation regions respectively. Our results are summarized in Section 5.

2 Leading-Twist Strangeness Production

The two component model we have used to study charm hadroproduction consists of a perturbative, leading-twist, component that normalizes the cross section at $x_F \sim 0$ and the intrinsic, higher-twist, component [17, 18, 19]. When addressing strangeness production, however, we must keep in mind that quarks lighter than charm are difficult to treat within the context of perturbative QCD. We thus choose a set of parton distribution functions that is most compatible with our needs and assume that the strange quark is massive, considering only the $gg \rightarrow s\overline{s}$ and $q\overline{q} \rightarrow s\overline{s}$ production channels.

Our treatment of strange quarks as heavy is rather uncertain since strange quarks are light, $m_s \approx 150 - 500$ MeV, and charm production is already subject to large corrections beyond leading order [21]. The lower end of the strange quark mass range is close to the $n_f = 3$ value of $\Lambda_{\rm QCD}$ and less than the initial scale of all parton distribution functions. The strong coupling constant will thus be large and the leading order (LO) cross section only a fraction of the complete result. Therefore a perturbative treatment of strange quark production is dubious. We will thus vary the normalization of the total leading-twist cross section to show the uncertainties in the absolute cross section.

The GRV 94 LO proton parton distribution functions [22] are most suitable because the strange quark distribution vanishes at the initial scale $Q_0^2 = 0.4$ GeV^2. The older GRV LO parton distribution functions [23] employ a lower initial scale but an isospin symmetric sea ($\overline{u} = \overline{d}$) while the most recent GRV 98 LO set [24] assumes a higher initial scale, $Q_0^2 = 0.8$ GeV^2. All other recent parton distribution functions [25] employ a scale of 1 GeV^2 or greater. We use the GRV LO pion set [26] for the pion parton distributions. We assume $m_s = 500$ MeV. This constituent quark value modulates α_s, keeping it below unity. In addition, to avoid going below Q_0^2, we assume that both α_s and the parton distributions are evaluated at scale $\mu = 2m_T = 2\sqrt{p_T^2 + m_s^2}$. The x_F distribution, obtained by integrating the differential partonic cross section over the p_T and rapidity, y, of the unobserved quark, selects low p_T.

A LO calculation provides the basic shape of the x_F distribution. The shape does not change significantly at higher orders, at least to next-to-leading order for charm and bottom quarks [27]. We will assume that this is also true for strange quarks. We further assume that the factorization theorem [28, 29, 30, 31] still holds for perturbative production of strange quarks.

We prefer to treat the strange quark as heavy rather than as a massless parton in hard $2 \rightarrow 2$ scatterings, "jet-like" processes. There are several reasons for this. First, treating the strange quark as a "jet" means selecting a minimum p_T to keep the cross section finite. A large minimum p_T compatible with hard scattering is incompatible with the assumption of intrinsic production, inherently a low p_T process [17]. A jet with a leading strange particle can be produced from all $2 \rightarrow 2$ processes in which a strange quark appears in the final state. However, strange particles can also be produced from the fragmentation of light quark and gluon jets. In any case, there is no indication that the strange particles measured by E791 originate from jets.

The x_F distribution of leading-twist production [32] of heavy quarks by gg fusion and $q\overline{q}$ annihilation is

$$H = \frac{d\sigma_{\rm lt}^S}{dx_F} = \frac{\sqrt{s}}{2} \int dz_3\, dy_2\, dp_T^2 \frac{1}{E_1} \frac{D_{S/s}(z_3)}{z_3}\, x_a x_b \Bigg(\sum_{q=u,d,s} \Big[f_q^A(x_a,\mu^2) f_{\overline{q}}^B(x_b,\mu^2) + f_{\overline{q}}^A(x_a,\mu^2) f_q^B(x_b,\mu^2) \Big] \frac{d\widehat{\sigma}_{q\overline{q}}}{d\hat{t}} + f_g^A(x_a,\mu^2) f_g^B(x_b,\mu^2) \frac{d\widehat{\sigma}_{gg}}{d\hat{t}} \Bigg) \, , \quad (1)$$

where a and b are the projectile and target partons, 1 and 2 are the produced strange quarks, and 3 is the final-state strange hadron S. Feynman x is defined as $x_F = 2(m_T/\sqrt{s})\sinh y$ where $\sqrt{s}$ is the hadron-proton center of mass energy. The leading order subprocess cross sections for heavy quark production can be found in Ref. [33]. The fractional momenta carried by the projectile and target partons, x_a and x_b, are $x_a = (m_T/\sqrt{s})(e^y + e^{y_2})$ and $x_b = (m_T/\sqrt{s})(e^{-y} + e^{-y_2})$ at LO with two massive quarks in the final state. The strange quark contribution is negligible, less than 0.1%. We equate $d\sigma_{\rm lt}^S/dx_F$ with H, the hard scattering cross section as a useful abbreviation.

The fragmentation functions, $D_{S/s}(z)$, describe the hadronization of the strange quark into strange hadron S. Since including the unknown strange quark fragmentation functions would only add an additional degree of uncertainty, we assume that

$$D_{S/s}(z) = B_S \delta(1-z) \; . \quad (2)$$

A delta function for fragmentation is in agreement with low p_T charm hadroproduction, see Ref. [32]. If all ten ground state strange hadrons are produced at the same rate, the normalization, B_S, is 0.1. We may overestimate the production of some strange hadrons in this way.

The LO x_F distribution for $\pi^- p$ interactions at 500 GeV, the energy of E791 [12, 13], are shown in Fig. 1. No K factors are included. The forward $\pi^- p$ cross section is rather hard, mostly due to the harder pion gluon distribution.

Although we have treated the strange quark as massive, we have also checked how the x_F distribution would change if the strange quark was treated as massless and all $2 \rightarrow 2$ scattering channels with an s quark in the final state were included. Generally, the additional "jet" production of strangeness is through processes such as $gs \rightarrow gs$ and $qs \rightarrow qs$ ($\overline{q}s \rightarrow \overline{q}s$) as well as for the $\overline{s}$. Including these "jet-like" processes increases the cross section by a factor of $4 - 8$. While this factor is not constant, it increases rather slowly with x_F so that the difference in shape is only important at large x_F where the cross section is decreasing more rapidly.

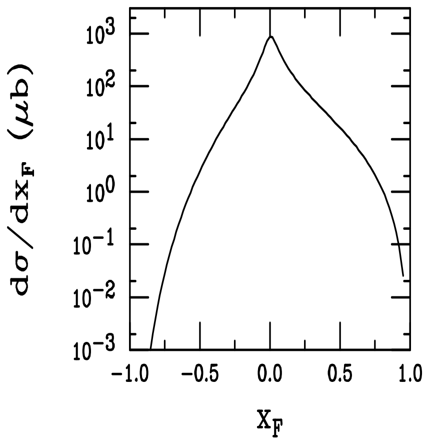

Figure 1: Strange quark production by leading-twist fusion in $\pi^- p$ interactions at 500 GeV.

3 Intrinsic Particle Production

The wavefunction of a hadron in QCD can be represented as a superposition of Fock state fluctuations, *e.g.* $|n_v\rangle$, $|n_v q\overline{q}\rangle$, $|n_v s\overline{s}\rangle$, $|n_v s\overline{s} q\overline{q}\rangle$ ...components where n_v are the valence quarks of the hadron. The additional $Q\overline{Q}$ pairs are said to be "intrinsic" to the hadron wavefunction. When the projectile scatters with the target, the coherence of the Fock state is broken and the intrinsic fluctuation can hadronize. This hadronization can proceed either by uncorrelated fragmentation, as in leading twist production, or by coalescence with spectator quarks in the wavefunction [15, 16, 34]. The generic intrinsic $Q\overline{Q}$ components are generated by virtual interactions such as $gg \rightarrow Q\overline{Q}$ where the gluons couple to two or more projectile valence quarks. The Fock states are dominated by configurations with equal rapidity constituents so that the quarks in an intrinsic state carry a larger fraction of the parent hadron momentum [15, 16]. The momentum boost received by the quarks in an intrinsic state depends on their mass and the number of partons in the Fock state probed.

We will calculate strange particle production from $\pi^-(\overline{u}d) + p(uud)$ interactions. At $x_F > 0$ the intrinsic fluctuations arise in the pion while at $x_F < 0$, the proton fragmentation region, the proton can be considered the source of intrinsic fluctuations. We assume no strange particle production by interference between the π^- and p Fock states.

The probability for an n–particle Fock state is taken to be frame-independent and may be written as [15, 16]

$$\frac{dP^n_{\rm iQ}}{dx_i \cdots dx_n} = N_n \frac{\delta(1 - \sum_{i=1}^n x_i)}{(m_h^2 - \sum_{i=1}^n (\widehat{m}_i^2/x_i))^2} \ . \tag{3}$$

where the subscript "iQ" denotes any generic Fock state with an arbitrary number, r, of intrinsic quark-antiquark pairs. The pairs could be light, strange, or heavy. If the hadron has n_v valence quarks, then the number of particles in the state is $n = n_v + 2r$. The probability is normalized by N_n where $n = 4$ and 5 for the minimal $|n_v s\overline{s}\rangle$ Fock configurations in a pion and a proton respectively. We consider initial hadron Fock states with up to $r = 3$ intrinsic pairs or $n = 8$ for mesons and 9 for baryons. The delta function in the numerator of Eq. (3) conserves longitudinal momentum. The dominant Fock configurations are closest to the light-cone energy shell and therefore the invariant mass, $M^2 = \sum_i \widehat{m}_i^2/x_i$, is minimized. The kinematic variables of the $i^{\rm th}$ particle in the state are the effective transverse mass squared, $\widehat{m}_i^2 = \langle \vec{k}_{T,i}^2\rangle + m_i^2$, and x_i is the light-cone momentum fraction. Assuming $\langle \vec{k}_{T,i}^2\rangle$ is proportional to the square of the constituent quark mass, we choose $\widehat{m}_q = 0.45$ GeV and $\widehat{m}_s = 0.71$ GeV [32, 35].

There are two possible ways of producing strange hadrons in the intrinsic model. Both require the presence of either a strange valence quark or at least one intrinsic $s\overline{s}$ pair in the Fock state configuration. Strange particles may be produced by uncorrelated fragmentation of a strange quark in the Fock state, as previously discussed for leading-twist strangeness production in Section 2. No strange hadrons are assumed to be produced by fragmentation of the light quarks. More importantly, the strange quark can hadronize through coalescence with spectator partons. If coalescence occurs in the minimal $|n_v s\overline{s}\rangle$ Fock state flavor correlations are introduced between the projectile and the final-state hadron, giving rise to a leading particle effect. While coalescence can still occur in higher-n Fock states, the flavor correlations are weaker and the leading particle effect less important. In fact, when $r = 3$ both the strange and antistrange hadrons can be produced by coalescence, giving no leading particle effect.

Uncorrelated fragmentation does not favor the production of one strange hadron over any other. No other valence quarks from the final-state hadron are necessary to produce a strange hadron by uncorrelated fragmentation. We assume equal probabilities for all ground state strange hadrons, independent of their mass and quark content, as in the treatment of strange particle production at leading twist. We allow strange quarks to fragment into strange hadrons and strange antiquarks to fragment into antistrange hadrons. We ignore strange particle production by fragmentation of other light quarks in the configuration. In this case, if the strange quark fragments into a kaon, the K distribution is

$$\frac{dP_{\rm iQ}^{nF}}{dx_F} = \int dz \prod_{i=1}^{n} dx_i \frac{dP_{\rm iQ}^{n}}{dx_1 \ldots dx_n} \frac{D_{K/s}(z)}{z} \delta(x_F - z x_s) \ . \tag{4}$$

The same distribution is thus valid for all strange particles produced by uncorrelated fragmentation from a given n-particle state. The fragmentation function from leading-twist production, Eq. (2), is also used here.

If the energy denominator is minimized in Eq. (3), as required for the intrinsic state to maintain its integrity, fragmentation may cost more energy than is available to produce the final-state strange particle. We will therefore test the importance of the fragmentation mechanism in the intrinsic state by comparing to strange hadron production with $P_{\rm iQ}^{nF} = 0$.

For a strange hadron, S, to be produced by coalescence, all the valence partons of S must be present in the Fock state. Since the multi-particle Fock states are fragile, they can easily coalesce into strange hadrons in high-energy, low momentum transfer reactions. No binding or mass effects are assumed. The coalescence contribution to strange hadron production is then

$$\frac{dP_{\rm iQ}^{nC}}{dx_F} = \int \prod_{i=1}^{n} dx_i \frac{dP_{\rm iQ}^{n}}{dx_1 \ldots dx_n} \delta(x_F - \sum_{m_v} x_{S_{m_v}}) \tag{5}$$

where $m = 2$ for mesons and three for baryons. The coalescence function is simply a delta function combining the momentum fractions of the valence quarks of the strange hadron present in the Fock state configuration. It is clear that only a small fraction of the strange hadrons can be produced from the minimal configuration with $r = 1$ ($n = 5$ for protons). However, coalescence can also occur within Fock state fluctuations with $r > 1$. Coalescence is calculated the same way in these higher configurations.

Since we wish to study the x_F distributions of all ground state strange and antistrange hadrons and the asymmetries between them, we include Fock state configurations with up to $r = 3$. Thus we include all possible light quark/strange quark combinations in Fock states with $n = 9$ for a proton and with $n = 8$ for a pion, allowing coalescence production of Ω and $\overline{\Omega}$. The minimum number of partons needed to produce a given ground state strange hadron by coalescence is shown in Table 1 along with the required combination of $Q\overline{Q}$ pairs for coalescence production.

We now discuss how the probability for the Fock states with $r = 1-3$ are determined. To remain close to the spirit of the original intrinsic charm model, we assume that $P_{\rm is}^5$ and higher Fock state probabilities can be obtained from $P_{\rm ic}^5$ by mass scaling, as in Ref. [19]. A reanalysis of the EMC charm structure function data with next-to-leading order calculations of charm electroproduction by both leading-twist photon-gluon fusion and higher-twist intrinsic charm was shown to be consistent with an intrinsic charm component in the proton at large $x_{\rm Bj}$ of $\approx 1\%$ or less [20]. (See also Ref. [36].) An earlier analysis found $P_{\rm ic}^5 = 0.31\%$ [37, 38]. To be conservative in our estimates of the intrinsic contribution to strange particle production, we will always assume that the total probability for a charm quark to arise from an $|n_v c\overline{c}\rangle$ state is 0.31% [20, 37, 38], regardless of the projectile identity, $P_{\rm ic}^5 = P_{\rm ic}^4$ for baryons and mesons. We scale $P_{\rm ic}^5$ by the square of the quark transverse masses to obtain

$$P_{\rm is}^5 \;\; = \;\; \left(\frac{\widehat{m}_c}{\widehat{m}_s}\right)^2 P_{\rm ic}^5 \approx 2\% \tag{6}$$

with $\widehat{m}_c = 1.8$ GeV [35]. The assumption that $P_{\rm ic}^5 = P_{\rm ic}^4$ leads to $P_{\rm is}^5 = P_{\rm is}^4$.

To normalize the probability of states with $r > 1$, we use the method described in Ref. [19]. Data on double charmonium hadroproduction were used to set an upper limit on the $|n_v c\overline{c}c\overline{c}\rangle$ probability: $P_{\rm icc}^7 \approx 0.044\ P_{\rm ic}^5$ [39]. Then the probabilities for Fock state

	Projectile	
Final State	$\pi^-(\overline{u}d)$	$p(uud)$
$K^-(\overline{u}s)$	$4(s\overline{s})$	$7(s\overline{s}u\overline{u})$
$\overline{K^0}(\overline{d}s)$	$6(s\overline{s}d\overline{d})$	$7(s\overline{s}d\overline{d})$
$\Lambda(uds)$	$6(s\overline{s}u\overline{u})$	$5(s\overline{s})$
$\Sigma^-(dds)$	$6(s\overline{s}d\overline{d})$	$7(s\overline{s}d\overline{d})$
$\Sigma^+(uus)$	$8(s\overline{s}u\overline{u}u\overline{u})$	$5(s\overline{s})$
$\Xi^0(uss)$	$8(s\overline{s}s\overline{s}u\overline{u})$	$7(s\overline{s}s\overline{s})$
$\Xi^-(dss)$	$6(s\overline{s}s\overline{s})$	$7(s\overline{s}s\overline{s})$
$\Omega(sss)$	$8(s\overline{s}s\overline{s}s\overline{s})$	$9(s\overline{s}s\overline{s}s\overline{s})$
$K^+(u\overline{s})$	$6(s\overline{s}u\overline{u})$	$5(s\overline{s})$
$K^0(d\overline{s})$	$4(s\overline{s})$	$5(s\overline{s})$
$\overline{\Lambda}(\overline{u}\overline{d}\overline{s})$	$6(u\overline{u}d\overline{d})$	$9(s\overline{s}u\overline{u}d\overline{d})$
$\overline{\Sigma^-}(\overline{d}\overline{d}\overline{s})$	$8(s\overline{s}d\overline{d}d\overline{d})$	$9(s\overline{s}d\overline{d}d\overline{d})$
$\overline{\Sigma^+}(\overline{uus})$	$6(s\overline{s}u\overline{u})$	$9(s\overline{s}u\overline{u}u\overline{u})$
$\overline{\Xi^0}(\overline{uss})$	$6(s\overline{s}s\overline{s})$	$9(s\overline{s}s\overline{s}u\overline{u})$
$\overline{\Xi^-}(\overline{d}\overline{ss})$	$8(s\overline{s}s\overline{s}d\overline{d})$	$9(s\overline{s}s\overline{s}d\overline{d})$
$\overline{\Omega}(\overline{sss})$	$8(s\overline{s}s\overline{s}s\overline{s})$	$9(s\overline{s}s\overline{s}s\overline{s})$

Table 1: The lowest number of partons in an intrinsic strangeness Fock state configuration for a strange hadron to be produced by coalescence.

configurations with $r = 2$ ($n = 7$ for a proton) can be fixed. We begin with [18]

$$P^7_{\rm icq} \approx \left(\frac{\widehat{m}_c}{\widehat{m}_q}\right)^2 P^7_{\rm icc} \ . \tag{7}$$

Then it follows that

$$\begin{aligned} P^7_{\rm isq} &= \left(\frac{\widehat{m}_c}{\widehat{m}_s}\right)^2 P^7_{\rm icq} = 0.704\, P^5_{\rm is} \ , & (8) \\ P^7_{\rm iss} &= \left(\frac{\widehat{m}_q}{\widehat{m}_s}\right)^2 P^7_{\rm isq} = 0.285\, P^5_{\rm is} \ . & (9) \end{aligned}$$

We take $P^7_{\rm isu} = P^7_{\rm isd}$. The relations in Eqs. (8)-(9) also hold for the $n = 6$ pion Fock states.

There is no guidance from intrinsic charm to normalize the Fock configurations with $r = 3$ since no triply-charm baryon distributions have been calculated. Thus we assume the same scaling between $P^9_{\rm issq}$ and $P^7_{\rm iss}$ as between $P^7_{\rm isq}$ and $P^5_{\rm is}$ in Eq. (8). Then

$$P^9_{\rm issq} = 0.704\, P^7_{\rm iss} = 0.2\, P^5_{\rm is} \ . \tag{10}$$

Mass scaling can then be used to obtain the other $r = 3$ ($n = 9$ for the proton) probabilities:

$$\begin{aligned} P^9_{\rm isss} &= \left(\frac{\widehat{m}_q}{\widehat{m}_s}\right)^2 P^9_{\rm issq} = 0.081\, P^5_{\rm is} \ , & (11) \\ P^9_{\rm isqq} &= \left(\frac{\widehat{m}_s}{\widehat{m}_q}\right)^2 P^9_{\rm issq} = 0.5\, P^5_{\rm is} \ , & (12) \end{aligned}$$

Note that here $P^9_{\rm issu} = P^9_{\rm issd}$ and $P^9_{\rm isuu} = P^9_{\rm isud} = P^9_{\rm isdd}$. In this case, we also assume the probabilities of the eight-particle Fock configurations are equal to their nine-particle counterparts given in Eqs. (10)-(12).

We have not included the probabilities for intrinsic states with only light quarks since these do not contribute to strange hadron production in pion and proton Fock states. If we consider hyperon beams like the Σ^-, these light intrinsic states would also contribute. The light intrinsic states must of course be considered when calculating the full probability sum,

$$P = \sum_{\rm Q} P^5_{\rm iQ} + \sum_{\rm Q,Q'} P^7_{\rm iQQ'} + \sum_{\rm Q,Q',Q''} P^9_{\rm iQQ'Q''} + \cdots \tag{13}$$

where $\mathrm{Q} = u, d, s, \cdots$. The total probability, $P = 1$, sets an upper bound on $P^5_{\rm is}$ since all other probabilities for lighter and heavier quarks can be related to it, see Eqs. (8)-(12). Considering only the light and strange quarks with $r = 1 - 3$, we find $P \approx 0.4$. The contributions from heavier quarks do not increase P significantly. The remainder of the hadron wavefunction would include multi-gluon as well as multiquark configurations which we have not included here. Thus $P^5_{\rm is}$ cannot be significantly increased to fit data.

The total intrinsic contribution to strange hadron production is a combination of uncorrelated fragmentation and coalescence. We do not consider production from configurations with $r > 3$. Recall that including still higher Fock states weakens the flavor correlations between the strange quarks and the valence quarks. In fact, only those strange hadrons produced in the Fock configuration with $r = 1$, such as the K^0, K^+, Λ and Σ^+ in the proton, are leading relative to the remaining strange hadrons. There will be an asymmetry between a Ξ^- in a $|uuds\overline{s}s\overline{s}\rangle$ state and a $\overline{\Xi^-}$ first produced in a $|uuds\overline{s}s\overline{s}d\overline{d}\rangle$ state, albeit not as strong. Since the relative probabilities decrease when additional pairs are added to the Fock state, further contributions, even including coalescence, will have only slightly different x_F distributions than those resulting from uncorrelated fragmentation in a configuration with lower n. There is then no longer any advantage in introducing more pairs into the configuration because the relative probability will decrease while the potential gain in momentum is not significant. However, for coalescence production of the Ω, all possible final-state strange hadrons from states with $r \leq 3$ are counted in the total intrinsic probability.

The unit-normalized probability distributions, $(1/P^n_{\rm iQ})(dP^n_{\rm iQ}/dx_F)$, for both uncorrelated fragmentation and coalescence are given in Appendix A. These probability distributions, when properly normalized and weighted, will comprise the intrinsic contribution to strange hadron production.

To calculate the full strange and antistrange hadron, S, x_F distributions in the intrinsic model, we include uncorrelated fragmentation of the strange quark in every state and coalescence from those states with the correct quark content. Since the intrinsic probability distributions and the coalescence mechanism are independent of the final-state mass, the results are identical for the ground state and higher strange resonances which have the same valence quarks. We have thus only taken the 10 ground state strange hadrons and antihadrons into account. To conserve uncorrelated fragmentation probability, we assume that $P^{nF}_{\rm iQ} = 0.1$. For the coalescence contribution, we count the number of possible ground state strange and antistrange hadron combinations that can be obtained from a given state. Each strange hadron or antihadron is assigned a weight, ξ, equivalent to the number of possible ways to produce that hadron from the total number of S or $\overline{S}$ hadrons in the state.

In general, the possible number of strange hadrons is greater than the number of possible antistrange hadrons in a given state. This has the effect of making, for example, $\overline{\Omega}$ production by coalescence more probable than the Ω in the proton since there are fewer antistrange hadrons in the final state. The overall effect is very small since both the Ω and $\overline{\Omega}$ are only produced from the $|uuds\overline{s}s\overline{s}s\overline{s}\rangle$ state. The appropriate x_F distribution from coalescence is weighted by the fraction of possible combinations of that final-state hadron to the total strange hadrons or antihadrons in each state. When a strange hadron can be produced by both fragmentation and coalescence, we take half the sum of the two contributions to conserve the total probability. If $P^{nF} \equiv 0$, only the coalescence weight obtained from counting contributes to the total probability.

Finally, to obtain the total probability of each strange hadron in the intrinsic model, we sum all the contributions from all the states. Thus

$$\frac{dP_S}{dx_F} = \sum_n \sum_{r_u} \sum_{r_d} \sum_{r_s} \beta \left(\frac{1}{10} \frac{dP^{nF}_{\mathrm{i}(r_s\mathrm{s})(r_u\mathrm{u})(r_d\mathrm{d})}}{dx_F} + \xi \frac{dP^{nC}_{\mathrm{i}(r_s\mathrm{s})(r_u\mathrm{u})(r_d\mathrm{d})}}{dx_F} \right) . \tag{14}$$

The weight of each state produced by coalescence is ξ where $\xi = 0$ when S cannot be produced by coalescence from state $|n_v r_s(s\overline{s}) r_u(u\overline{u}) r_d(d\overline{d})\rangle$. The parameter β is 1 when $\xi = 0$ and 0.5 when production by both fragmentation and coalescence is possible to conserve probability in each state. When we assume coalescence production only, $P^{nF} \equiv 0$ and $\beta \equiv 1$. The number of up, down and strange $Q\overline{Q}$ pairs is indicated by r_u, r_d and r_s respectively. The total, $r_u + r_d + r_s = r$, is defined as $r = (n - n_v)/2$ because each Q in an n-parton state is accompanied by a $\overline{Q}$. For baryon projectiles, $n = 5$, 7, and 9 while for mesons $n = 4$, 6, and 8. Depending on the value of n, r_i can be 0, 1, 2 or 3, *e.g.* in a $|uuds\overline{s}d\overline{d}d\overline{d}\rangle$ state, $r_u = 0$, $r_d = 2$ and $r_s = 1$ with $r = 3$. The detailed probability distributions for all strange and antistrange hadrons from the intrinsic states of the π^- and p are given in Appendix B.

This method of assigning the probabilities without regard for strange particle mass is, of course, quite simplistic, especially for production by independent fragmentation, but adequate for testing the general characteristics of the model. The only way that baryon number or strangeness number enters the calculation is through the choice of S. Other methods of calculating the relative production rates, such as including the mass in a statistical fashion, would not distinguish between strange and antistrange hadrons, as suggested by the data [12, 13]. Therefore we make the minimum number of assumptions to see if the general framework of the model is correct.

4 Model Predictions

We now turn to specific predictions of our model for the total strange and antistrange hadron distributions and the asymmetries between them. The x_F distribution for final-state strange hadron S is the sum of the leading-twist fusion and intrinsic components,

$$\frac{d\sigma^S_{hN}}{dx_F} = \frac{d\sigma^S_{\mathrm{lt}}}{dx_F} + \frac{d\sigma^S_{\mathrm{iQ}}}{dx_F} . \tag{15}$$

The normalization of the production cross section is determined by the Fock state probability, the inelastic hN cross section, and a scale factor set by the momentum needed to break the coherence of the Fock state. The total intrinsic cross section,

$d\sigma_{\rm iQ}^S/dx_F$, is related to dP_S/dx_F by

$$\frac{d\sigma_{\rm iQ}^S}{dx_F} = \sigma_{hN}^{\rm in} \frac{\mu^2}{4\widehat{m}_s^2} \frac{dP_S}{dx_F} \; . \tag{16}$$

The scale, μ^2, was fixed at 0.1 GeV^2 in intrinsic charm studies [19]. If $\mu^2 = 0.1$ as determined for intrinsic charm [19], $\sigma_{\rm ic} \approx 0.6$ μb for pions and 0.8 μb for protons assuming $P_{\rm ic}^5 = 0.3\%$. This value of μ^2 along with $P_{\rm is}^5 = 2\%$ gives $\sigma_{\rm is} \approx 0.24$ mb for pions and 0.3 mb for protons. The inelastic pN and $\pi^- N$ cross sections are taken from the Particle Data Group parameterizations [40] and are evaluated at $\sqrt{s'} = \sqrt{s}(1 - |x_F|)$ [18]. Recall that the total probability distributions, dP_S/dx_F, for each strange hadron S are given in Appendix B.

To distinguish between the scenarios with and without fragmentation, we will denote $d\sigma_{\rm iQ}^S/dx_F$ by $F + C$ for fragmentation and coalescence and C for coalescence alone. The total distributions from Eq. (15) are then $H + F + C$ and $H + C$ respectively. We will also attempt to fit the asymmetry data by scaling the leading-twist result relative to the intrinsic contribution, denoted by $H + aC$. Since we do not know which component should be rescaled, we discuss the consequences in each case. We also discuss alternative ways to fit the data. Finally, we show the asymmetries without leading-twist fusion or fragmentation, C only.

We give $d\sigma_{\rm iQ}^S/dx_F = F + C$ from $\pi^- p$ interactions at 500 GeV in Figs. 2 and 3. The results in Fig. 2 correspond to $x_F > 0$ while those in Fig. 3 correspond to $x_F < 0$. The distributions $d\sigma_{\rm iQ}^S/dx_F = C$ are given in Figs. 4 and 5. The energy dependence enters only through $\sigma_{hN}^{\rm in}$ which sets the relative normalization at $x_F \sim 0$. Some of the intrinsic distributions are equal for a given projectile. The largest number of distributions are related for the π^- since the pion has both a valence quark and a valence antiquark. Then,

$$\begin{array}{lll} \dfrac{d\sigma_{\rm iQ}^{K^-}}{dx_F} = \dfrac{d\sigma_{\rm iQ}^{K^0}}{dx_F} & & \dfrac{d\sigma_{\rm iQ}^{K^+}}{dx_F} = \dfrac{d\sigma_{\rm iQ}^{\overline{K^0}}}{dx_F} \\ \dfrac{d\sigma_{\rm iQ}^{\Lambda}}{dx_F} = \dfrac{d\sigma_{\rm iQ}^{\overline{\Lambda}}}{dx_F} = \dfrac{d\sigma_{\rm iQ}^{\Sigma^-}}{dx_F} = \dfrac{d\sigma_{\rm iQ}^{\overline{\Sigma^+}}}{dx_F} & & \dfrac{d\sigma_{\rm iQ}^{\Sigma^+}}{dx_F} = \dfrac{d\sigma_{\rm iQ}^{\overline{\Sigma^-}}}{dx_F} \\ \dfrac{d\sigma_{\rm iQ}^{\overline{\Xi^-}}}{dx_F} = \dfrac{d\sigma_{\rm iQ}^{\Xi^0}}{dx_F} & & \dfrac{d\sigma_{\rm iQ}^{\Xi^-}}{dx_F} = \dfrac{d\sigma_{\rm iQ}^{\overline{\Xi^0}}}{dx_F} \; . \end{array} \tag{17}$$

The relations in the left column of Eq. (17) are for "leading" particles with valence quarks in common with the projectile while those in the right column are "nonleading". In addition, $d\sigma_{\rm iQ}^{\Omega}/dx_F = d\sigma_{\rm iQ}^{\overline{\Omega}}/dx_F$. The antistrange hadron distributions from baryon projectiles are more likely than the strange hadron distributions to be the same since only strange hadrons can share valence quarks with the projectile. Thus, we find that

$$\frac{d\sigma_{\rm iQ}^{K^-}}{dx_F} = \frac{d\sigma_{\rm iQ}^{\overline{K^0}}}{dx_F}$$

$$
\begin{aligned}
\frac{d\sigma_{\rm iQ}^{\overline{\Sigma^-}}}{dx_F} &= \frac{d\sigma_{\rm iQ}^{\overline{\Sigma^+}}}{dx_F} = \frac{d\sigma_{\rm iQ}^{\overline{\Lambda}}}{dx_F} \\
\frac{d\sigma_{\rm iQ}^{\overline{\Xi^-}}}{dx_F} &= \frac{d\sigma_{\rm iQ}^{\overline{\Xi^0}}}{dx_F} \ .
\end{aligned}
\tag{18}
$$

for protons. All the equalities in Eq. (18) are for "nonleading" particles.

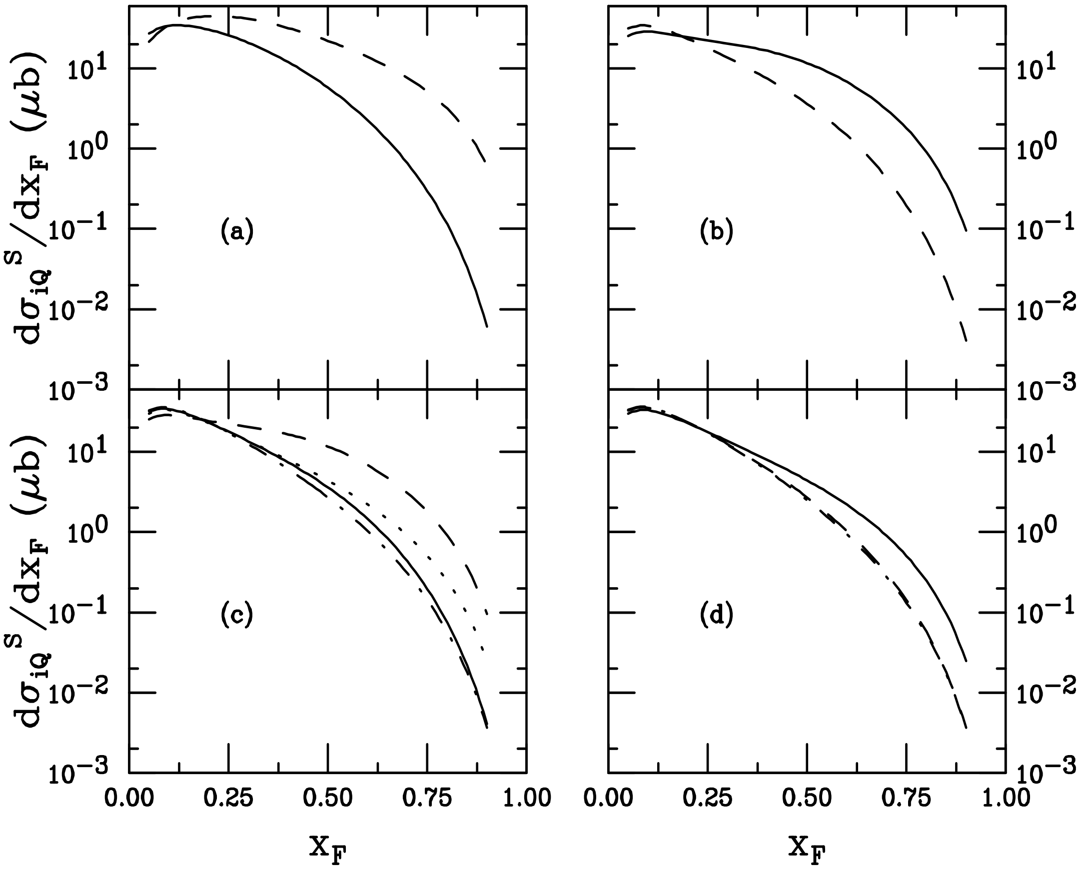

Figure 2: The total intrinsic strange and antistrange hadron production cross sections with a π^- projectile. (a) The solid curve is for $K^+ = \overline{K^0}$ and the dashed for $K^- = K^0$. (b) The $\Lambda = \overline{\Lambda} = \Sigma^-$ (solid) and $\overline{\Sigma^-}$ (dashed) distributions are given. (c) The Σ^+ (solid), $\overline{\Sigma^+}$ (dashed), Ξ^0 (dot-dashed), and $\overline{\Xi^0}$ (dotted) distributions are shown. (d) The Ξ^- (solid), $\overline{\Xi^-}$ (dashed) and $\Omega = \overline{\Omega}$ (dot-dashed) predictions are shown.

The $K^- = K^0$ distributions in Fig. 2(a) are the hardest strange hadron distributions from the π^-, as expected from Table 4. The $\Lambda\,(\Sigma^0)$, $\overline{\Lambda}$, Σ^- and $\overline{\Sigma^+}$ are the hardest strange baryon distributions, followed by the $\overline{\Xi^0}$ and Ξ^-. The pion-induced strange hadron distributions in Fig. 2 are all relatively harder than those from the proton, shown in Fig. 3. Due to the pion valence antiquark, the antistrange hadron distributions can sometimes be harder than the strange hadron distributions, compare the $\overline{\Sigma^+}$ and the Σ^+ distributions as well as the $\overline{\Xi^0}$ and the Ξ^0 distributions in Fig. 2(c).

The Λ in Fig. 3(b) and the Σ^+ in Fig. 3(c) have the hardest strange baryon distribu-

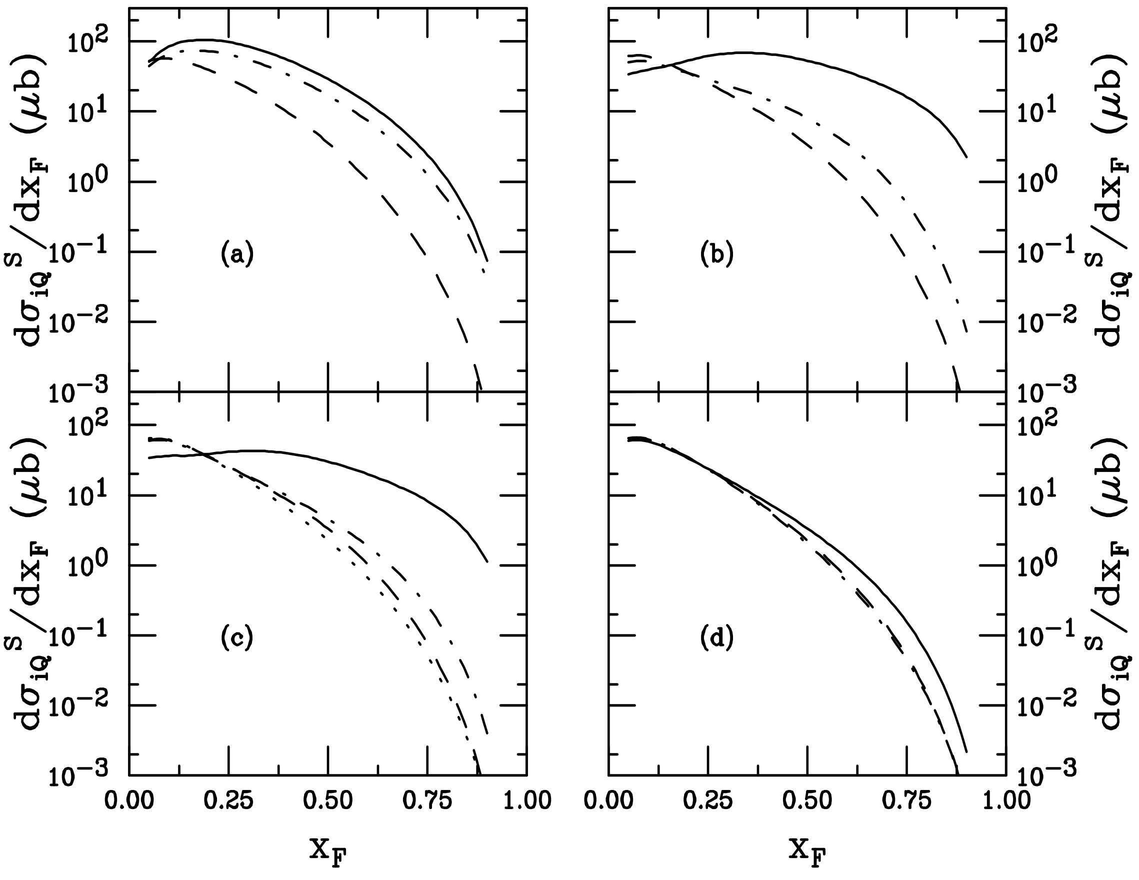

Figure 3: The total intrinsic strange and antistrange hadron production cross sections with a proton projectile. (a) The K^+ (solid), K^- (dashed), and K^0 (dot-dashed) calculations are presented. (b) The Λ (solid), $\overline{\Lambda}$ and $\overline{\Sigma^-}$ (dashed), and Σ^- (dot-dashed) distributions are given. (c) The Σ^+ (solid), $\overline{\Sigma^+}$ (dashed), Ξ^0 (dot-dashed), and $\overline{\Xi^0}$ (dotted) distributions are shown. (d) The Ξ^- (solid), $\overline{\Xi^-}$ (dashed), and Ω (dot-dashed) predictions are shown. The $\overline{\Omega}$ distribution is indistinguishable from the Ω distribution here even though the two are not identical.

tions in a proton projectile. The distributions are relatively flat because the final-state hadrons both share two valence quarks, ud and uu respectively, with the proton. Both can be produced from Fock states with $n = 5$. The Λ distribution is the hardest of the two since either of the two u valence quarks in the proton can be paired with the d in the minimal state while the pairing of the two u valence quarks can only happen once. The counting differences also occur in the higher Fock configurations, but then it is equally likely that the strange quark is paired with a valence or a sea quark since the model makes no distinction between their distributions. When only a single proton valence quark is shared with the final-state hadron, the average x_F in the intrinsic model is much lower, as can be seen in a comparison between the Λ and Σ^- distributions in Fig. 3(b). A comparison of the Ξ^0 distribution in Fig. 3(c) and the Ξ^- distribution in Fig. 3(d) shows that the combinatoric effect of two valence u quarks against a single valence d quark also affects the doubly strange baryons. The Ξ^0 distribution is harder than the Ξ^- even though neither can be produced in the minimal Fock configuration. Likewise, the K^+ and K^0 share a single valence quark with the proton. The combinatorial effect also holds for the mesons so that the K^+ has a harder distribution than the K^0, as seen in Fig. 3(a). The antistrange meson and baryon distributions are all similar.

The corresponding results with coalescence alone are shown in Figs. 4 and 5. Now the low to intermediate x_F fragmentation contributions are missing, resulting in much lower intrinsic contributions in that region. The relative normalization at high x_F also changes since including fragmentation reduces the coalescence contribution by a factor of two in Eq. (14) since $\beta = 0.5$ with fragmentation and $\beta = 1$ with coalescence alone. This can be seen, for example, in the Λ distribution in Fig. 4(b). On the other hand, leaving out fragmentation from states with $r = 1$ causes the x_F distributions of strange hadrons produced by coalescence only in Fock states with $r = 3$, such as the $\overline{\Sigma^+}$, to decrease more rapidly at high x_F because the tail of the fragmentation distribution from the $r = 1$ state gives a larger contribution at high x_F than coalescence from the $|\overline{u}ds\overline{s}u\overline{u}u\overline{u}\rangle$ state. These results are typical for all strange antibaryon distributions where coalescence can occur in only a single Fock state. In these cases, the intrinsic model x_F distribution is simply the corresponding distribution from Figs. 11-14 normalized to the cross section as in Eq. (16). Here the differences in the distributions due to the weight factors ξ in Eq. (14) are clearly visible, as seen in the separation between the Ω and $\overline{\Omega}$ distributions in Fig. 5(d).

Our complete results are the sum of the distributions shown in Figs. 2-5 with the leading-twist production in Fig. 1. A comparison of these figures shows the general trends we can expect for $d\sigma^S_{hN}/dx_F$ in Eq. (15). The intrinsic cross sections in Fig. 2 are about 100 times smaller than the leading twist cross section at $x_F \sim 0$ and would only become important for hadrons sharing valence quarks with the pion unless considerable rescaling is needed to fit the data.

It is often difficult to obtain high statistics on single hadron distributions, especially at large x_F. Therefore, a more quantitative way to study very similar strange hadron

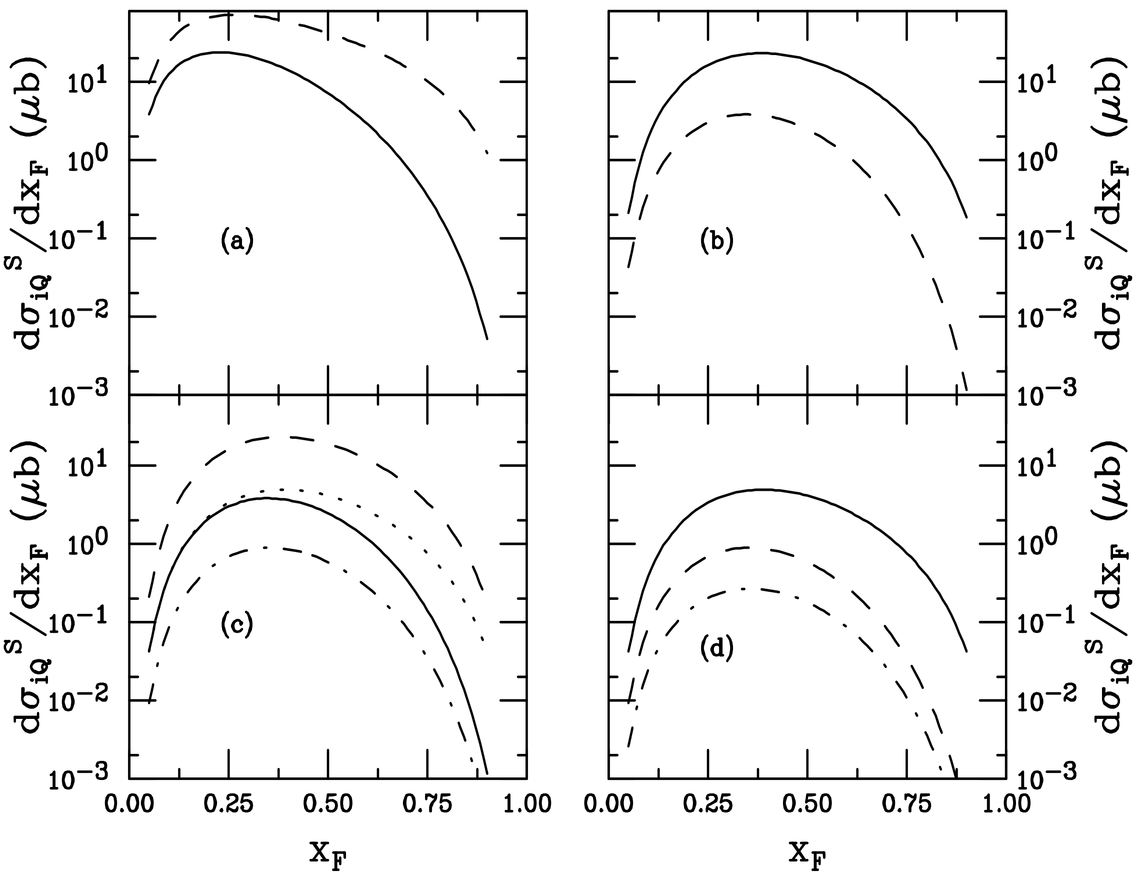

Figure 4: The total intrinsic strange and antistrange hadron production cross sections with a π^- projectile including coalescence only. (a) The solid curve is for $K^+ = \overline{K^0}$ and the dashed for $K^- = K^0$. (b) The $\Lambda = \overline{\Lambda} = \Sigma^-$ (solid) and $\overline{\Sigma^-}$ (dashed) distributions are given. (c) The Σ^+ (solid), $\overline{\Sigma^+}$ (dashed), Ξ^0 (dot-dashed), and $\overline{\Xi^0}$ (dotted) distributions are shown. (d) The Ξ^- (solid), $\overline{\Xi^-}$ (dashed) and $\Omega = \overline{\Omega}$ (dot-dashed) predictions are shown.

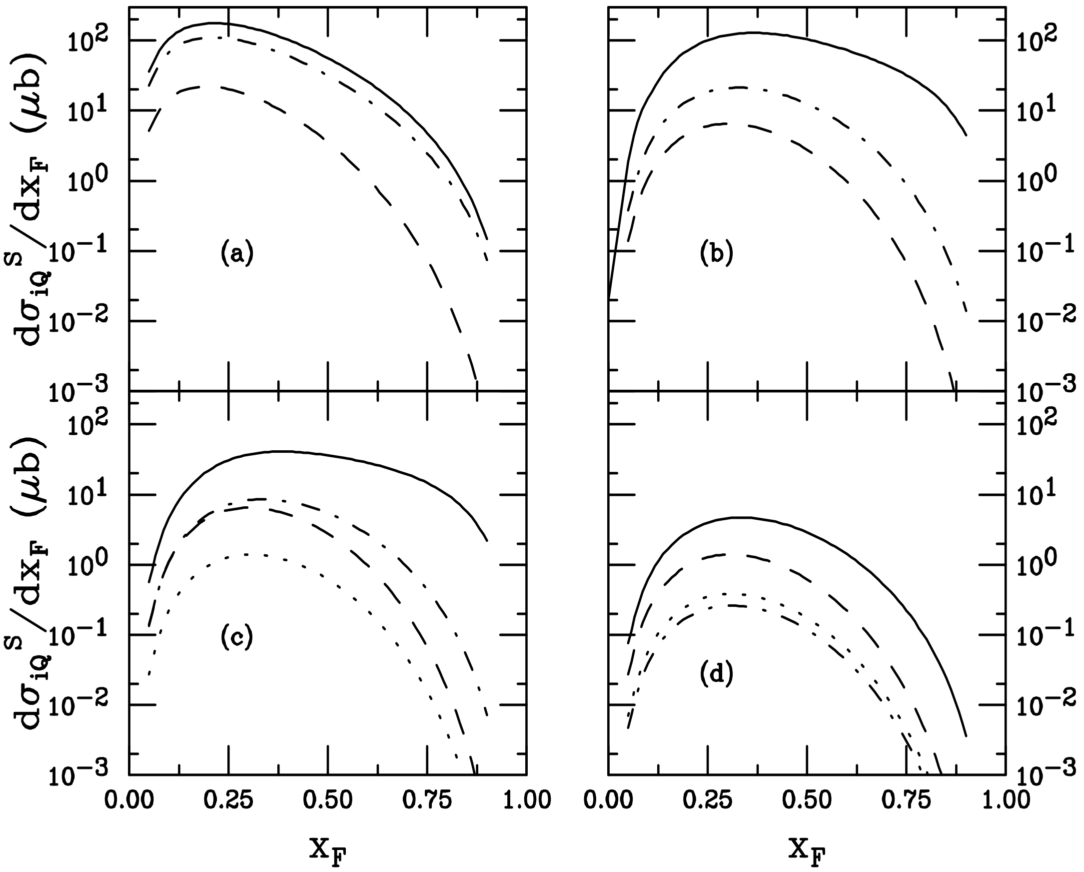

Figure 5: The total intrinsic strange and antistrange hadron production cross sections with a proton projectile including coalescence only. (a) The K^+ (solid), K^- (dashed), and K^0 (dot-dashed) calculations are presented. (b) The Λ (solid), $\overline{\Lambda}$ and $\overline{\Sigma^-}$ (dashed), and Σ^- (dot-dashed) distributions are given. (c) The Σ^+ (solid), $\overline{\Sigma^+}$ (dashed), Ξ^0 (dot-dashed), and $\overline{\Xi^0}$ (dotted) distributions are shown. (d) The Ξ^- (solid), $\overline{\Xi^-}$ (dashed), Ω (dot-dashed), and $\overline{\Omega}$ (dotted) predictions are shown.

distributions is through the asymmetry, defined as

$$A_S(x_F) = \frac{d\sigma^S/dx_F - d\sigma^{\overline{S}}/dx_F}{d\sigma^S/dx_F + d\sigma^{\overline{S}}/dx_F} \tag{19}$$

where again S represents a strange hadron and $\overline{S}$ its antistrange counterpart. Note that we choose to form the asymmetry between strange and antistrange hadrons rather than defining "leading" and "nonleading" particles for each projectile because the definition of "leading" may change from one projectile to another. For example, the $K^+(u\overline{s})$ is leading in the proton but not in the π^- since the π^- has no valence u quark.

The asymmetries A_Λ, A_{Ξ^-}, and A_Ω have been measured in π^--induced interactions at 500 GeV [12, 13]. The measurements are around $|x_F| < 0.1$. In the forward direction, $x_F > 0$, A_Λ and A_Ω are independent of x_F with $A_\Lambda \approx A_\Omega \approx 0.1$ while A_{Ξ^-} increases with x_F to $A_{\Xi^-} \approx 0.2$. On the other hand, at negative x_F, only A_Ω is independent of x_F. The other asymmetries increase as x_F decreases, approaching $A_\Lambda \approx 0.4$ and $A_{\Xi^-} \approx 0.3$ at $x_F = -0.1$. The data are inconsistent with PYTHIA which produces essentially no asymmetry between the particle/antiparticle combinations at forward x_F while at negative x_F, only A_Λ is increasing significantly although less rapidly than the data [12, 13]. At negative x_F, A_{Ξ^-} remains small while A_Ω becomes negative. Note that even if PYTHIA was tuned to reproduce the asymmetries at $x_F \approx 0$, the behavior would remain inconsistent with the data. On the other hand, the trends of the data are consistent with recombination models which predict $A_\Lambda > A_{\Xi^-} > A_\Omega$ at negative x_F and $A_{\Xi^-} > A_\Lambda \sim A_\Omega$ at forward x_F [12, 13]. The coalescence contributions to the intrinsic model have the same general trends as the recombination model. However, the distributions may differ in detail.

We can compare our model calculations with the E791 results. In the case of a π^- projectile, positive x_F is the beam fragmentation region and, in the intrinsic model, the strange hadrons are intrinsic to the pion. Negative x_F corresponds to the target fragmentation region which is modeled as intrinsic production from a proton. Thus to form the asymmetry at negative x_F, we take the proton-induced intrinsic probability distributions and sum these with the $\pi^- p$ leading-twist calculation. We therefore give results in each x_F region separately.

An asymmetry of ~ 0.14 at $x_F \sim 0$, as seen by E791 [12, 13], suggests that the strange baryon production cross sections are about 30% larger than those of antistrange baryons. This initial asymmetry between baryons and antibaryons at leading twist could arise from associated production of strange baryons with antistrange kaons, for example $\pi^- p \to \Sigma^+ K^0 \pi^-$, $\Lambda K^+ \pi^-$, or $\Sigma^- K^+ \pi^0$. Thus strange baryon production only requires that one or more kaons be produced to conserve strangeness and baryon number. However, when an antistrange baryon is produced, both strangeness and baryon number conservation require at least two baryons[2] to be produced with it, for example $\pi^- p \to \Lambda \overline{\Lambda} n$. These additional baryons increase the kinetic energy threshold by 3.5 GeV

[2]The baryons need not be strange if kaons are also produced.

[41]. The beam energy may not be high enough for the increased energy threshold of antistrange baryon production to be neglected. In this situation, it is easy to imagine a 30% or greater strange baryon and/or antistrange kaon enhancement which manifests itself as a nonzero asymmetry at $x_F \sim 0$.

To check how well our model can reproduce the trends of the data without tuning, we have assumed that the leading twist fusion cross section is 30% larger for all strange relative to antistrange baryons. We also assume that, because $K^+(u\overline{s})$ and $K^0(d\overline{s})$ production is favored by associated production over $K^-(\overline{u}s)$ and $\overline{K^0}(\overline{d}s)$, the K^+ and K^0 cross sections are also 30% larger than the K^- and $\overline{K^0}$. This is more reasonable than forcing exact strangeness conservation in the model because the $\pi^- p \rightarrow K^0 \overline{K^0} n$ kinetic threshold is only 360 MeV greater than that of the $\Lambda K^+ \pi^-$ final state and $K\overline{K}$ pair production would moderate the K^0 over $\overline{K^0}$ enhancement from strangeness conservation. There is then no exact strangeness conservation in our perturbative leading-twist calculation. Since a model of the exclusive strangeness production channels is inherently nonperturbative, it is beyond the scope of our leading-twist calculation. Therefore an assumption of an overall asymmetry of 30% for strange baryons and antistrange mesons is more reasonable than assuming exact strangeness conservation without a complete knowledge of the associated production channels. Therefore the real A_S may change 10-20% at $x_F \approx 0$ with energy and final-state particle.

On the other hand, exact strangeness conservation is required in the intrinsic model since s and $\overline{s}$ quarks must be added to the Fock state in pairs. Baryon production by coalescence is naturally favored over antibaryon production in the intrinsic model, as seen by inspection of Eqs. (B.2)-(B.33). No other initial asymmetry need be considered. Therefore, we assume an initial asymmetry only in the leading-twist calculation.

We first present the asymmetries for $\pi^- p$ interactions at 500 GeV in Figs. 6 and 7. In the pion fragmentation region, A_{K^-}, A_{Σ^+}, and A_{Ξ^0} are all negative at large x_F due to the $\overline{u}$ valence quark in the π^- except when no leading-twist contribution is included. Note that A_{K^-} is largest because the K^- can be produced by coalescence already in the minimum Fock state configuration. The next largest asymmetry is A_{Σ^+} while A_{Ξ^0} is the weakest. The decrease in the asymmetry is due to both the lower probabilities of the higher Fock states and the reduced average x_F for a doubly strange hadron. On the other hand, $A_{\overline{K^0}}$, A_{Σ^-}, and A_{Ξ^-} are all positive, reflecting the d valence quark of the π^-. The trends of the asymmetries are the same as those particle/antiparticle pairs with negative asymmetries.

Observe that A_Λ and A_Ω are virtually flat and would be exactly zero if we had assumed either exact strangeness conservation for both the leading twist and the intrinsic calculations or an initial asymmetry between strange and antistrange hadrons in both models. The fact that the asymmetry decreases with x_F is because the assumed 30% difference between the particle and antiparticle cross sections in the leading-twist calculation becomes less important as x_F increases and the intrinsic contribution begins to dominate.

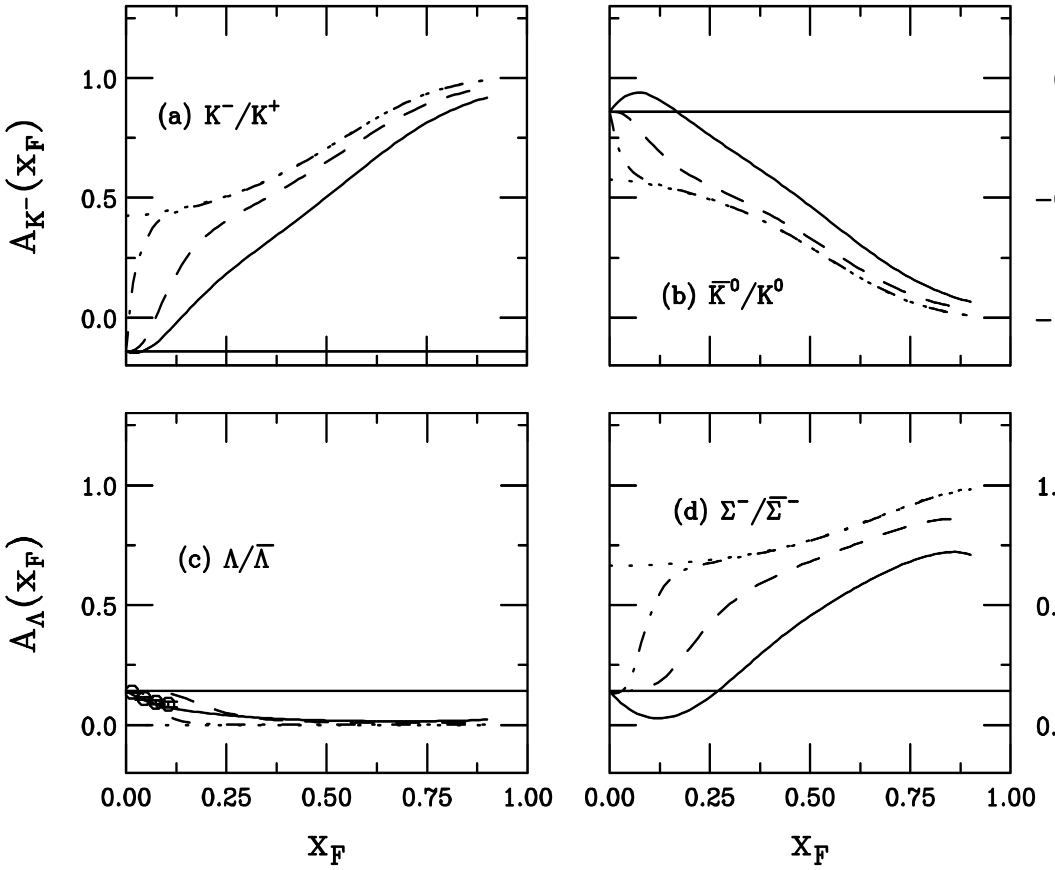

Figure 6: Model asymmetries for $\pi^- p$ interactions at 500 GeV with $H + F + C$ (solid), $H + C$ (dashed), $H + aC$ (dot-dashed) and C alone (dotted) are shown for (a) A_{K^-}, (b) $A_{\overline{K^0}}$, (c) A_Λ and (d) A_{Σ^-}. The horizontal solid curve is the asymmetry from leading-twist production alone. The E791 data [12, 13] on A_Λ are also shown.

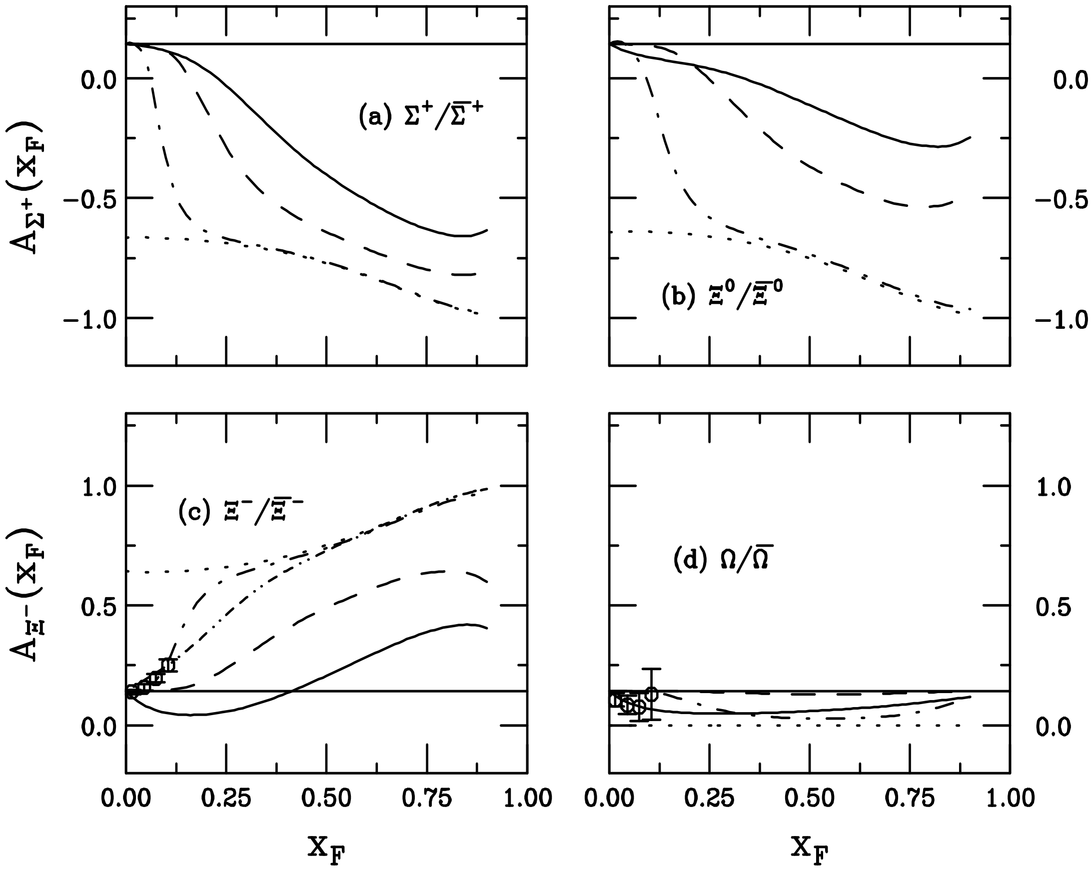

Figure 7: Model asymmetries for $\pi^- p$ interactions at 500 GeV with $H + F + C$ (solid), $H + C$ (dashed), $H + aC$ (dot-dashed) and C alone (dotted) are shown for (a) A_{Σ^+}, (b) A_{Ξ^0}, (c) A_{Ξ^-} and (d) A_Ω. The result with the modified $\overline{\Xi^-}$ distributions is shown in the dot-dot-dash-dashed curve in (c). The horizontal solid curve is the asymmetry from leading-twist production alone. The E791 data [12, 13] on A_{Ξ^-} and A_Ω are also shown.

We also note that even though, for example in Figs. 2 and 4, the intrinsic K^+ and $\overline{K^0}$ x_F distributions are equal and the K^- and K^0 x_F distributions are equal, $|A_{K^-}|$ and $|A_{\overline{K^0}}|$ are not equal. This is because the particle/antiparticle enhancement factor of 1.3 is applied to the K^+ and K^0, resulting in different asymmetries at low x_F. We find the same differences at low x_F between A_{Σ^-} and A_{Σ^+} as well as between A_{Ξ^0} and A_{Ξ^-}.

We now compare the results with $H + F + C$ and $H + C$. As noted earlier, when the intrinsic state is assumed to undergo independent fragmentation as at leading-twist, the probability for the final state strange hadron to be produced within any Fock state is evenly divided between fragmentation and coalescence to conserve probability, hence $\beta = 0.5$ in Eq. (14). This division results in a "dip" in the asymmetry at low x_F, as seen for example in A_{Σ^-} in Fig. 6(d). (Similar results were observed for charm hadron asymmetries, see Ref. [17].) Thus, turning off intrinsic fragmentation has the general result of increasing the asymmetry more rapidly at low x_F. The effect is largest for A_{K^-} and $A_{\overline{K^0}}$ since the K^- and K^0 are both produced in the lowest state with $n = 4$. For particles produced by coalescence in higher Fock states, the increase is slower, such as for A_{Ξ^-} in Fig. 9(c). Since the Ξ^- is first produced by coalescence in the $|\overline{u}ds\overline{s}s\overline{s}\rangle$ state, the asymmetry does not begin to increase until $x_F > 0.1$. This rather slow turn on is not in accord with the E791 data but is in better agreement with the data than the calculations including intrinsic-model fragmentation. The A_Λ and A_Ω results do not change significantly if fragmentation is neglected in the intrinsic model. Thus, the results in Figs. 6 and 7 reflect the general trend of the E791 data but A_{Ξ^-} does not increase as rapidly as the data, even with intrinsic-model fragmentation turned off.

Regardless of whether or not fragmentation is included does not significantly affect the agreement of our calculations with the data for A_Λ and A_Ω. However, it is clear that the "dip" in A_{Ξ^-} caused by fragmentation goes in the opposite direction from the data. Even leaving fragmentation out does not cause A_{Ξ^-} to increase at low x_F. Thus to find agreement with this data, we rescale the intrinsic contribution, $H + aC$. We could equally well rescale the fusion while leaving the intrinsic fixed to achieve the same effect. Choosing $a = 40$ gives the agreement shown in the dot-dashed curves. Comparing this result to that with the asymmetry in the intrinsic model with C only shows that by $x_F \sim 0.4$, the $H + aC$ result behaves like that with C alone. At this point, the relative intrinsic contribution is large enough to produce a second peak in the x_F distribution of $H + aC$, as seen in PYTHIA calculations of charm hadrons, see Ref. [19]. This convergence of the two results appears at lower x_F for singly strange baryons and K mesons, $x_F \sim 0.25$ and 0.10 respectively. Only in these more extreme cases does $A_S \to 1$ for most strange hadrons.

In Table 2, we give $\langle x_F \rangle$ for all particles and antiparticles at $x_F > 0$. Generally, antistrange hadrons have a larger $\langle x_F \rangle$ than their corresponding strange hadron. This occurs because the strange hadron distribution at leading twist is larger by a uniform 30% over all x_F. The multiplication makes the leading twist hadron distribution higher at low x_F and the antihadron x_F distributions do not fall steeply enough when fragmentation is included for the average x_F of strange particles to be larger than those for antistrange

Final State	$H+F+C$	$H+C$	$H+aC$	C only
$K^-(\overline{u}s)$	0.259	0.307	0.357	0.359
$\overline{K^0}(\overline{d}s)$	0.178	0.201	0.286	0.291
$\Lambda(uds)$	0.200	0.253	0.411	0.420
$\Sigma^-(dds)$	0.200	0.253	0.411	0.420
$\Sigma^+(uus)$	0.152	0.144	0.332	0.378
$\Xi^0(uss)$	0.147	0.124	0.256	0.381
$\Xi^-(dss)$	0.158	0.163	0.386	0.425
$\Omega(sss)$	0.145	0.119	0.184	0.384
$K^+(u\overline{s})$	0.170	0.189	0.285	0.291
$K^0(d\overline{s})$	0.246	0.292	0.357	0.359
$\overline{\Lambda}(\overline{uds})$	0.211	0.275	0.414	0.420
$\overline{\Sigma^-}(\overline{dds})$	0.158	0.152	0.342	0.378
$\overline{\Sigma^+}(\overline{uus})$	0.211	0.275	0.414	0.420
$\overline{\Xi^0}(\overline{uss})$	0.165	0.175	0.395	0.425
$\overline{\Xi^-}(\overline{dss})$	0.152	0.126	0.274	0.381
$\overline{\Omega}(\overline{sss})$	0.150	0.120	0.199	0.384

Table 2: The average x_F for strange hadrons produced at $x_F > 0$ in $\pi^- p$ collisions at 500 GeV for all cases considered. The average x_F for H alone is 0.117.

particles. The Ξ^- is an exception because it is leading relative to the $\overline{\Xi^-}$. All the others are either equally leading or nonleading.

In general, $\langle x_F \rangle$ increases between the cases with $H+F+C$ and $H+C$. However, for Σ^+, Ξ^0, Ω, $\overline{\Sigma^-}$, $\overline{\Xi^-}$, and $\overline{\Omega}$, $\langle x_F \rangle$ without fragmentation is less than that with $H+F+C$. The drop occurs because these particles are all produced by coalescence only in $n = 8$ states so that eliminating the fragmentation contribution considerably reduces the overall probability, thus reducing $\langle x_F \rangle$, compare Figs. 2 and 4. Rescaling the relative cross sections, $H + aC$, generally increases $\langle x_F \rangle$ considerably, from 20% for K^- and K^0 to more than a factor of two for the states first produced when $n = 8$, as could be expected by the existence of a second peak in some of the distributions. The increase in $\langle x_F \rangle$ between $H + aC$ and C alone is quite small in some cases, particularly for particles produced in Fock states with $n = 4$ and 6. The averages for K^- and $\overline{K^0}$, the only hadrons produced from $n = 4$ states, increase by less than 1%. Hadrons first produced with $n = 6$, $\overline{K^0}$, K^+, Λ, $\overline{\Lambda}$, Σ^-, $\overline{\Sigma^+}$, Ξ^-, and $\overline{\Xi^0}$, show an increase in $\langle x_F \rangle$ of 2-10%. The other hadrons, produced only when $n = 8$ increase somewhat more. The Ω and $\overline{\Omega}$ show an exceptionally large increase in $\langle x_F \rangle$, a factor of two, between $H + aC$ and C only. This large effect is because even when the intrinsic contribution is enhanced by a factor of 40 the leading-twist cross section is still dominant. Also, comparison of the C only results for $\langle x_F \rangle$ of Ω and $\overline{\Omega}$ show that they agree with $\langle x_F \rangle$ of the $|\overline{u}ds\overline{s}s\overline{s}s\overline{s}\rangle$ state in Table 4, as expected. The same is true for other hadrons only produced from a single

$n = 8$ state. Possible small differences may arise because while the intrinsic probability is energy-independent, the cross section is proportional to $\sigma h N^{\rm inel}(\sqrt{s'})$ evaluated at $\sqrt{s}(1 - |x_F|)$.

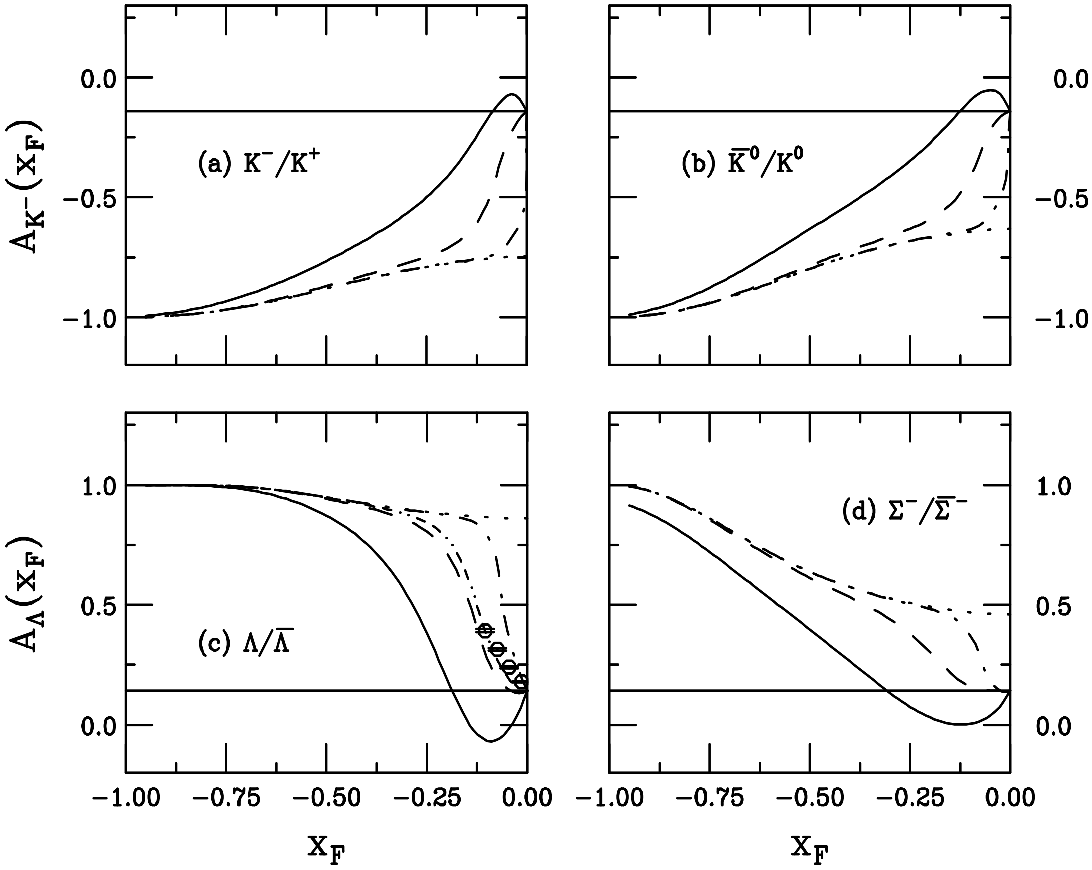

Figure 8: symmetries for $\pi^- p$ interactions at 500 GeV with $H + F + C$ (solid), $H + C$ (dashed), $H + aC$ (dot-dashed) and C alone (dotted) are shown for (a) A_{K^-}, (b) $A_{\overline{K^0}}$, (c) A_Λ and (d) A_{Σ^-}. The result with the modified $\overline{\Lambda}$ distributions is shown in the dot-dot-dash-dashed curve in (c). The horizontal solid curve is the asymmetry from leading-twist production alone. The E791 data [12, 13] on A_Λ are also shown.

In Figs. 8 and 9, we show the corresponding model calculations at negative x_F. Now all asymmetries are positive at large x_F, as might be expected from the target fragmentation region, typically a proton in a light target. The fastest increase in the asymmetry is for A_Λ and A_{Σ^+} which both have two valence quarks in common with the proton. The next largest strange/antistrange baryon asymmetry is A_{Σ^-} because the Σ^- has a single strange quark and shares only one valence quark with the proton. The doubly strange baryon asymmetries are somewhat weaker with $A_{\Xi^0} > A_{\Xi^-}$ because Ξ^0 coalescence production is more probable since the proton has two u valence quarks and only one d valence quark. This is the same reason why A_{K^-} is somewhat larger than $A_{\overline{K^0}}$ at intermediate x_F. Finally, A_Ω is negligible.

Turning fragmentation off is shown to significantly increase the asymmetries at low

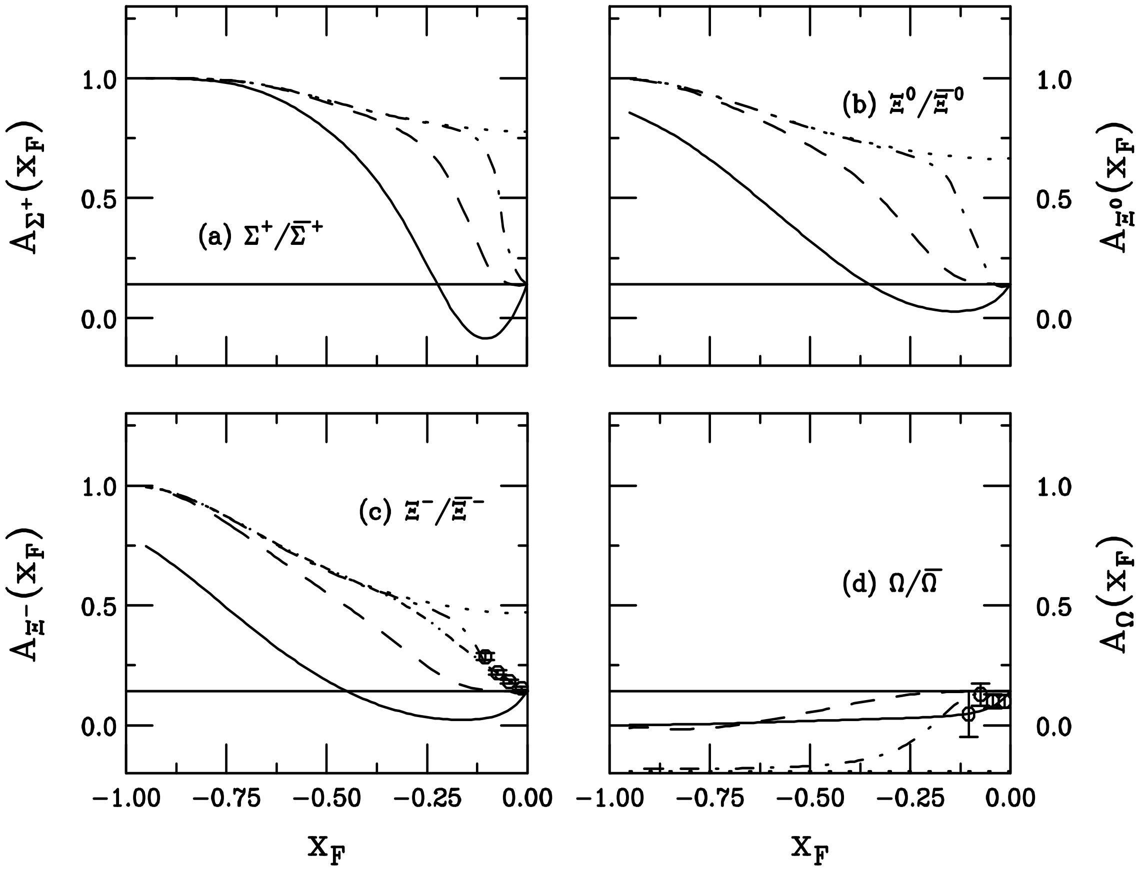

Figure 9: Model asymmetries for $\pi^- p$ interactions at 500 GeV with $H + F + C$ (solid), $H + C$ (dashed), $H + aC$ (dot-dashed) and C alone (dotted) are shown for (a) A_{Σ^+}, (b) A_{Ξ^0}, (c) A_{Ξ^-} and (d) A_Ω. The result with the modified $\overline{\Xi^-}$ distributions is shown in the dot-dot-dash-dashed curve in (c). The horizontal solid curve is the asymmetry from leading-twist production alone. The E791 A_{Ξ^-} and A_Ω data [12, 13] are also shown.

$|x_F|$, even more so than in the pion fragmentation region in Figs. 6 and 7. The effect is particularly strong for A_Λ where the "dip" due to probability conservation for fragmentation and coalescence causes the asymmetry to become negative for $|x_F| < 0.15$. The dip disappears when fragmentation is turned off and A_Λ increases rapidly already at $|x_F| \geq 0$ since the Λ is produced by coalescence already in the $|uuds\overline{s}\rangle$ state. However, this rapid turn on still does not increase A_Λ as quickly as the data. The same slower turn on in A_{Ξ^-} without fragmentation seen in Fig. 7(c) is also seen here.

Note also that for $H+C$, at large $|x_F|$ all $A_S \rightarrow 1$ except A_Ω since fragmentation not only builds up the low to moderate x_F intrinsic contribution but also tends to mask the effects of coalescence in higher Fock states. Thus $A_{\Xi^-} < 1$ at large $|x_F|$ with $H+F+C$ but $A_{\Xi^-} \sim 1$ at high $|x_F|$ for $H+C$ because the Ξ^- is already produced in the seven-particle $|uuds\overline{s}s\overline{s}\rangle$ state while the $\overline{\Xi^-}$ is only produced in the nine-particle $|uuds\overline{s}s\overline{s}d\overline{d}\rangle$ state. When both strange hadrons are only produced from the same Fock state, as is the case for the Ω and $\overline{\Omega}$, the asymmetry is small and nearly independent of x_F since only the relative weight factors are different.

Similar to the $x_F > 0$ results shown in Figs. 6 and 7, these calculations reflect the trends of the data but do not increase fast enough to reproduce it in detail, even for $H + C$. Therefore we have also calculated the asymmetries with the same scale factor, $a = 40$, used to fit A_{Ξ^-} in Fig. 7. While the agreement with A_{Ξ^-} in Fig. 9 is also quite good, the scaled result significantly overestimates A_Λ. The scaled results converge to those with C only even more rapidly than at forward x_F since the decrease in the leading twist cross section is more rapid due to the steeper gluon distribution in the proton. The exception is for A_Ω where the different weights for Ω and $\overline{\Omega}$ result in an overall negative asymmetry. The different weights also account for the fact that $A_{\Sigma^+} > A_{\Sigma^-}$ and $A_{\Xi^0} > A_{\Xi^-}$ at $x_F \sim 0$ with C alone. The Σ^+ and Ξ^0 have greater weights since they share u valence quarks with the proton.

The average x_F values of the $\pi^- p$ calculations at negative x_F are given in Table 3. The absolute values of these averages are generally smaller than those in Table 2. This is due in part to the more steeply falling x_F distribution at $x_F < 0$ in Fig. 1 which reflects the gluon distribution in the proton. The nonleading averages agree according to Eq. (18), as expected.

The data seem to indicate that uncorrelated fragmentation from the intrinsic state is ruled out, possibly due to the energy cost from a nearly on-shell Fock state. Not only is fragmentation ruled out, but the increase in A_{Ξ^-} seems to require a very strong coalescence contribution relative to the leading-twist result. We now examine this possibility in more detail.

While we have rescaled the intrinsic contribution, it is not necessarily clear which component should indeed be changed. Obviously the intrinsic probability cannot be increased by such a large factor–it would clearly exceed the probability sum, $P = 1$, in Eq. (13). The only other parameter in the intrinsic calculation is μ^2, the scale at which

Final State	$H+F+C$	$H+C$	$H+aC$	C only
$K^-(\overline{u}s)$	-0.142	-0.152	-0.248	-0.254
$\overline{K^0}(\overline{d}s)$	-0.142	-0.152	-0.248	-0.254
$\Lambda(uds)$	-0.303	-0.372	-0.433	-0.435
$\Sigma^-(dds)$	-0.153	-0.190	-0.357	-0.368
$\Sigma^+(uus)$	-0.254	-0.332	-0.434	-0.427
$\Xi^0(uss)$	-0.134	-0.140	-0.350	-0.377
$\Xi^-(dss)$	-0.128	-0.116	-0.329	-0.374
$\Omega(sss)$	-0.120	-0.082	-0.137	-0.343
$K^+(u\overline{s})$	-0.222	-0.258	-0.292	-0.293
$K^0(d\overline{s})$	-0.196	-0.236	-0.285	-0.287
$\overline{\Lambda}(\overline{u}\overline{d}\overline{s})$	-0.134	-0.128	-0.311	-0.337
$\overline{\Sigma^-}(\overline{dds})$	-0.134	-0.128	-0.311	-0.337
$\overline{\Sigma^+}(\overline{uus})$	-0.134	-0.128	-0.311	-0.337
$\overline{\Xi^0}(\overline{uss})$	-0.127	-0.093	-0.252	-0.340
$\overline{\Xi^-}(\overline{dss})$	-0.127	-0.093	-0.252	-0.340
$\overline{\Omega}(\overline{sss})$	-0.126	-0.084	-0.172	-0.343

Table 3: The average x_F for strange hadrons produced at $x_F < 0$ in $\pi^- p$ collisions at 500 GeV in all our scenarios. The average x_F for H alone is -0.081.

the coherence of the Fock state is broken. Increasing μ^2 by a factor of 40 would give an unacceptably large intrinsic cross section, $\sigma_{\rm is} = 9$ and 13 mb for π^- and p interactions respectively, $\sim$ 40% of the inelastic cross section. Such a large cross section seems unlikely. On the leading-twist side, the parameter B_S in the fragmentation function, Eq. (2), could be different for different final states. We assumed $B_S = 0.1$ for all final states. However, as discussed previously, the relative rates between K, Λ, Σ, Ξ and Ω production are unknown. It could well be that B_S should be considerably smaller for doubly-strange baryons than we have chosen. Taking a slightly larger B_S for Λ production could account for the overestimate of A_Λ with rescaling.

The asymmetries alone do not provide enough information about the individual cross sections. A comparison of the inclusive x_F distributions with the model over a broader range of x_F is essential to check whether there is any indication of a second peak at intermediate x_F. In Fig. 10 we show the individual x_F distributions that are used in the asymmetry calculations in each case. There is data on Ξ^- production by pion and neutron beams on nuclear targets [42, 43] at lower energies that are consistent with the relatively small intrinsic component in Eq. (6). In fact, the shapes of the measured x_F distributions agree with both the $H+F+C$ and $H+C$ results, showing no evidence for an enhancement at intermediate x_F.

Since rescaling as in $H + aC$ is inconsistent with the measured Ξ^- distributions

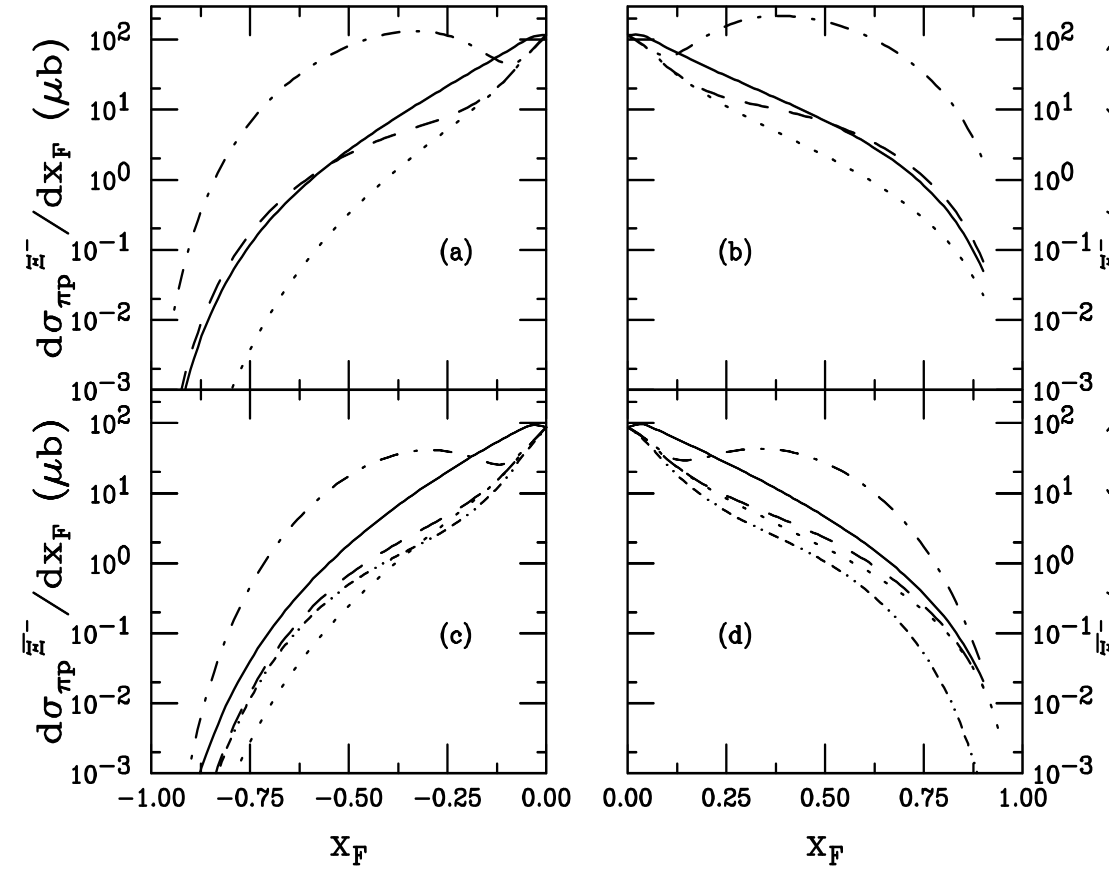

Figure 10: The model Ξ^- x_F distributions in the proton (a) and pion (b) fragmentation regions and the $\overline{\Xi^-}$ x_F distributions in the proton (c) and pion (d). The curves show the results for $H + F + C$ (solid), $H + C$ (dashed), $H + aC$ (dot-dashed) and H alone (dotted) are shown for both Ξ^- and $\overline{\Xi^-}$. The modified $\overline{\Xi^-}$ distributions are shown in the dot-dot-dash-dashed curves in (c) and (d).

over a larger range of x_F than that covered by the asymmetries, we have also checked another possibility–that the leading-twist distribution of strange particles is modified for those hadrons not sharing at least one valence quark with the "projectile" (the pion at $x_F > 0$ and the proton at $x_F < 0$). This modification would retain the agreement of the model with the Ξ^- x_F distributions while modifying the asymmetries. At $x_F > 0$, A_{Ξ^-} would be affected but because both the Ω and $\overline{\Omega}$ distributions would be modified simultaneously, leaving A_Ω unchanged. A_Λ would also be unaffected since both the Λ and $\overline{\Lambda}$ share a valence quark with the π^-. The other asymmetries in the forward direction would change. In the negative x_F region, all the asymmetries would be affected except A_Ω. The assumption that the leading-twist cross section for hadrons not sharing a valence quark with the "projectile" is modified so that $H \to H' = H(1-x_F)^2$ agrees very well with A_{Ξ^-} in Figs. 7 and 9 and with A_Λ in Fig. 8, as shown in the dot-dot-dash-dashed curves. With this assumption, A_{Ξ^-} rises more slowly than the $H + aC$ calculations but follows the asymptotic behavior of $H + aC$ and C only at similar values of x_F. In Fig. 10(c), the difference between the $H + C$ and $H' + C$ curves is rather small for $|x_F| < 0.5$ where the intrinsic contribution dominates. At low $|x_F|$, the $H' + C$ distribution lies below the dotted curve with H alone and it is in this region where the rapid growth of the asymmetry takes place. In Fig. 10(d), the hard leading-twist distribution is only slightly below the calculated $H + C$ result so that the modification $H \to H'$ puts the $H' + C$ curve lower than that with H alone over the entire x_F range.

While a modification of the leading-twist distribution for "nonleading" hadrons is fairly ad hoc it is the one scenario that agrees with the available strangeness data [12, 13, 42, 43]. Therefore any strong enhancement of the intrinsic contribution is ruled out. However, the absence of an intrinsic contribution seems to be ruled out also since, in such a case, $A_\Lambda = A_{\Xi^-}$ at $x_F < 0$, clearly incompatible with the data. There is no evidence for modification of the leading-twist charm distributions since the D^+ x_F distribution in $\pi^- N$ interactions is consistent with perturbative QCD. The case for perturbative production of strangeness is much weaker so that it is difficult to rule out such a change. To either verify or disprove such a modification, the x_F distribution of the antistrange hadrons should be measured with sufficient accuracy.

Finally, we point out that we have assumed proton targets in all cases. If we assume a nuclear target and take into account both neutrons and protons in the target fragmentation region, the differences between, for example, A_{K^-} and $A_{\overline{K^0}}$ would disappear if the target had an equal number of neutrons and protons. In addition, the intrinsic model predicts that the A dependence should be weaker than linear, $A^{0.71}$ for protons and $A^{0.77}$ for pions [35]. Thus the asymmetries would decrease at intermediate values of x_F for nuclear targets. We will study strange particle production as a function of x_F on nuclear targets [42, 43] in a future work [44].

5 Summary and Conclusions

We have extended the intrinsic charm model of Refs. [17, 18, 32] to strange hadrons. We have inferred the probabilities for the Fock states with 1-3 intrinsic $Q\overline{Q}$ pairs. We calculated the strange hadron distributions predicted in the intrinsic model for $\pi^- p$ interactions. We find that the model predicts asymmetries at lower values of x_F than for the more massive charm quarks. We correctly produce the general trends of the $\pi^- p$ data but not the strong increase of the asymmetry at low $|x_F|$, even when intrinsic-model fragmentation is switched off. The data are suggestive that fragmentation is not effective in the intrinsic model. The increase in the asymmetries A_{Ξ^-} and A_Λ with x_F cannot be reproduced in the model unless either the intrinsic cross section is increased greatly or the shape of the leading-twist nonleading distribution is modified. Increasing the intrinsic cross section to obtain agreement with the asymmetries modifies the individual x_F distributions too strongly, destroying agreement with inclusive Ξ^- spectra [42, 43]. Modifying the leading-twist distribution is consistent with all data so far but the inclusive x_F distributions of $\overline{\Xi^-}$ are unavailable. We have also shown that the modified leading-twist distribution alone cannot describe the asymmetries since then A_Λ and A_{Ξ^-} should then be identical in the proton fragmentation region. Precision data are clearly needed, particularly on the antistrange baryon x_F distributions, to test these hypotheses

It would thus be interesting to evaluate the asymmetries for other particles and other projectile types to further test the intrinsic model.

Acknowledgments: We thank J.C. Anjos, S.J. Brodsky, J. Engelfried, G. Herrera, P. Hoyer, E. Ramberg and J. Rathsman for discussions. R.V. would like to thank the Geschellschaft für Schwerionenforschung and the Niels Bohr Institute for hospitality during the completion of this work.

References

[1] E.M. Aitala *et al.* (E791 Collab.), Phys. Lett. **B371** (1996) 157.

[2] M. Aguilar-Benitez *et al.* (LEBC-EHS Collab.), Phys. Lett. **161B** (1985) 400.

[3] M. Aguilar-Benitez *et al.* (LEBC-EHS Collab.), Z. Phys. **C31** (1986) 491

[4] S. Barlag *et al.* (ACCMOR Collab.), Z. Phys. **C49** (1991) 555.

[5] M.I. Adamovich *et al.* (WA82 Collab.), Phys. Lett. **B305** (1993) 402.

[6] G.A. Alves *et al.* (E769 Collab.), Phys. Rev. Lett. **72** (1994) 812.

[7] R. Werding (WA89 Collab.), in Proceedings of *ICHEP94*, 27$^{\text{th}}$ International Conference on High Energy Physics, Glasgow, Scotland (1994).

[8] M.I. Adamovich *et al.* (WA89 Collab.), Eur. Phys. J. **C8** (1999) 593.

[9] E. Ramberg (SELEX Collab.), in *Hyperons, Charm and Beauty Hadrons*, Proceedings of the 2$^{\text{nd}}$ International Conference on Hyperons, Charm and Beauty Hadrons, Montreal, Canada, 1996, edited by C.S. Kalman *et al.*, Nucl. Phys. **B** (Proc. Suppl.) **55A** (1997) 173.

[10] J. Engelfried *et al.*, in Proceedings of the 5$^{\text{th}}$ Workshop on Heavy Quarks at Fixed Target, Rio de Janeiro, Brazil, 2000, hep-ex/0012004.

[11] E.M. Aitala *et al.* (E791 Collab.), Phys. Lett. **B411** (1997) 230.

[12] J.C. Anjos and E. Cuautle, in Proceedings of the *Seventh Mexican Workshop on Particle and Fields*, edited by A. Ayala, G. Contreras, and G. Herrera, AIP, New York, 2000, p. 172.

[13] E.M. Aitala *et al.* (E791 Collab.), Phys. Lett. **B496** (2000) 9.

[14] T. Sjöstrand, Comput. Phys. Commun. **82** (1994) 74. Program updates and documentation can be found at *http://www.thep.lu.se/tf2/staff/torbjorn/Pythia.html*.

[15] S.J. Brodsky, P. Hoyer, C. Peterson and N. Sakai, Phys. Lett. **B93** (1980) 451.

[16] S. J. Brodsky, C. Peterson and N. Sakai, Phys. Rev. **D23** (1981) 2745.

[17] R. Vogt and S.J. Brodsky, Nucl. Phys. **B438** (1995) 261.

[18] R. Vogt and S.J. Brodsky, Nucl. Phys. **B478** (1996) 311.

[19] T. Gutierrez and R. Vogt, Nucl. Phys. **B539** (1999) 189.

[20] B.W. Harris, J. Smith, and R. Vogt, Nucl. Phys. **B461** (1996) 181.

[21] J. Smith and R. Vogt, Z. Phys. **C75** (1997) 271.

[22] M. Glück, E. Reya, A. Vogt, Z. Phys. **C67** (1995) 433.

[23] M. Glück, E. Reya, and A. Vogt, Z. Phys. **C53** 127, (1992).

[24] M. Glück, E. Reya, and A. Vogt, Eur. Phys. J. **C5** (1998) 461.

[25] H. Plothow-Besch, 'PDFLIB: Proton, Pion and Photon Parton Density Functions, Parton Density Functions of the Nucleus, and α_s Calculations', Users's Manual - Version 8.04, W5051 PDFLIB, 2000.04.17, CERN-ETT/TT.

[26] M. Glück, E. Reya, and A. Vogt, Z. Phys. **C53** (1992) 651.

[27] R. Vogt, Z. Phys. **C71** (1996) 475.

[28] J.C. Collins, D.E. Soper and G. Sterman, *Perturbative QCD*, ed. A.H. Mueller (World Scientific, Singapore, 1989).

[29] G. Bodwin, Phys. Rev. **D31** (1985) 2616, **D34** (1986) 3932.

[30] J. Qiu and G. Sterman, Nucl. Phys. **B353** (1991) 105.

[31] J. Qiu and G. Sterman, Nucl. Phys. **B353** (1991) 137.

[32] R. Vogt, S.J. Brodsky and P. Hoyer, Nucl. Phys. **B383** (1992) 643.

[33] R.K. Ellis, in *Physics at the 100 GeV Scale*, Proceedings of the 17$^{\rm th}$ SLAC Summer Institute, Stanford, California, 1989, edited by E.C. Brennan (SLAC Report No. 361) 45.

[34] S.J. Brodsky, P. Hoyer, A.H. Mueller and W.-K. Tang, Nucl. Phys. **B369** (1992) 519.

[35] R. Vogt, S.J. Brodsky and P. Hoyer, Nucl. Phys. **B360** (1991) 67.

[36] F.M. Steffens, W. Melnitchouk, and A.W. Thomas, Eur. Phys. J. **C11** (1999) 673.

[37] J.J. Aubert *et al.* (EM Collab.), Phys. Lett. **110B** (1982) 73.

[38] E. Hoffmann and R. Moore, Z. Phys. **C20** (1983) 71.

[39] R. Vogt and S.J. Brodsky, Phys. Lett. **B349** (1995) 569.

[40] C. Caso *et al.*, Eur. Phys. J. **C3** 1, (1998).

[41] A. Capella, U. Sukhatme, C.I. Tan and J. Tran Thanh Van, Phys. Rev. **D36** (1987) 109.

[42] S.F. Biagi *et al.*, Z. Phys. **C34** (1987) 187.

[43] M.I. Adamovich *et al.* (WA89 Collab.), Z. Phys. **C76** (1997) 35.

[44] T.D. Gutierrez and R. Vogt, in preparation.

Appendix A

In this appendix, we show the normalized probability distributions $(1/P^n_{\rm iQ})(dP^n_{\rm iQ}/dx_F)$, for both uncorrelated fragmentation and coalescence are given for the pion and proton Fock states in Figs. 11-14. These probability distributions, when properly weighted, will comprise the intrinsic contribution to strange hadron production. The probability distributions for pions from Fock states with $n = 4$, 6 and 8 are given in Figs. 11 and 12. Figures 13 and 14 are the corresponding intrinsic probability distributions from Fock states with $n = 5$, 7 and 9.

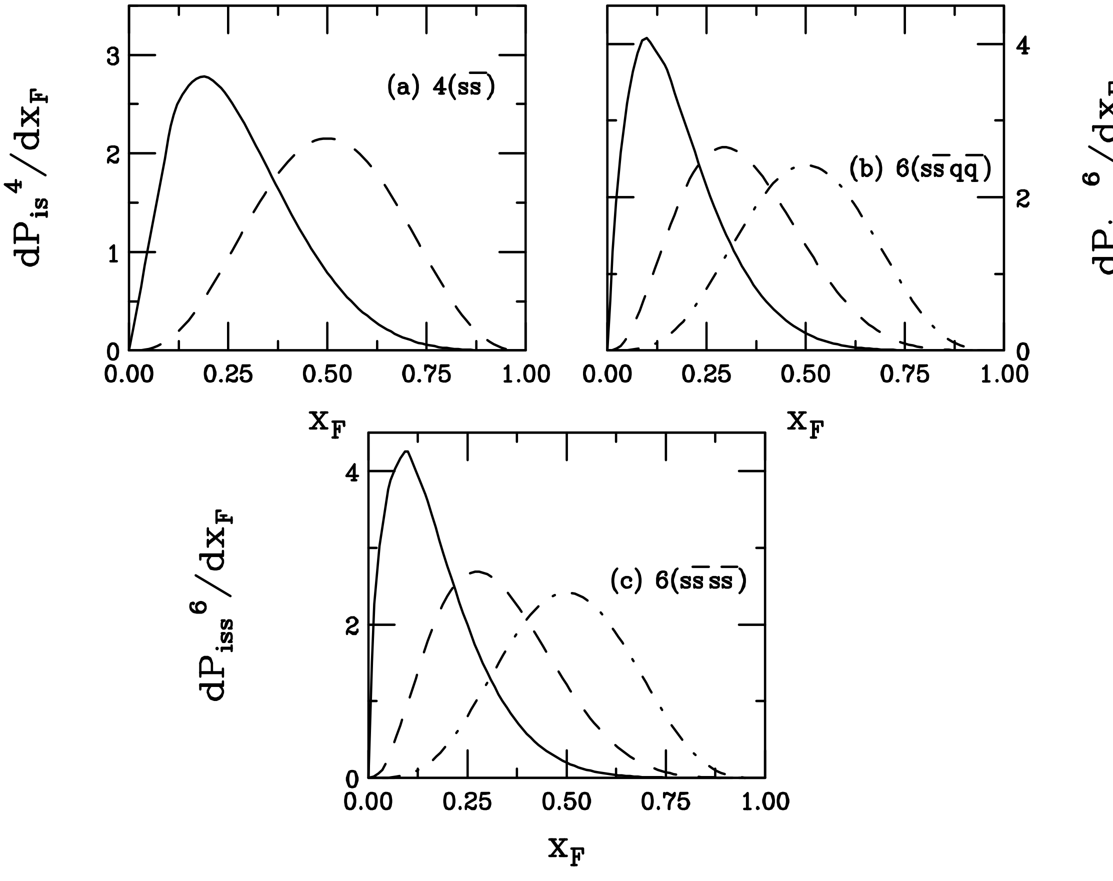

Figure 11: Strange hadron production in the intrinsic model from a π^- projectile in a minimal 4-particle $s\bar{s}$ Fock state, (a), a 6-particle Fock state with light quark pair, $q = u$ or d, and one $s\bar{s}$ pair, (b), and with two $s\bar{s}$ pairs (c). Both the uncorrelated fragmentation and coalescence distributions are shown. The solid curve in each case is the strange quark distribution, equivalent to the hadron distribution from uncorrelated fragmentation. The other curves are the probability distributions for hadron production by coalescence. The dashed curves are the K meson distributions. The dot-dashed curve in (b) is the baryon or antibaryon distribution with a single $s/\bar{s}$ quark while the dot-dashed curve in (c) is the doubly-strange baryon/antibaryon distribution.

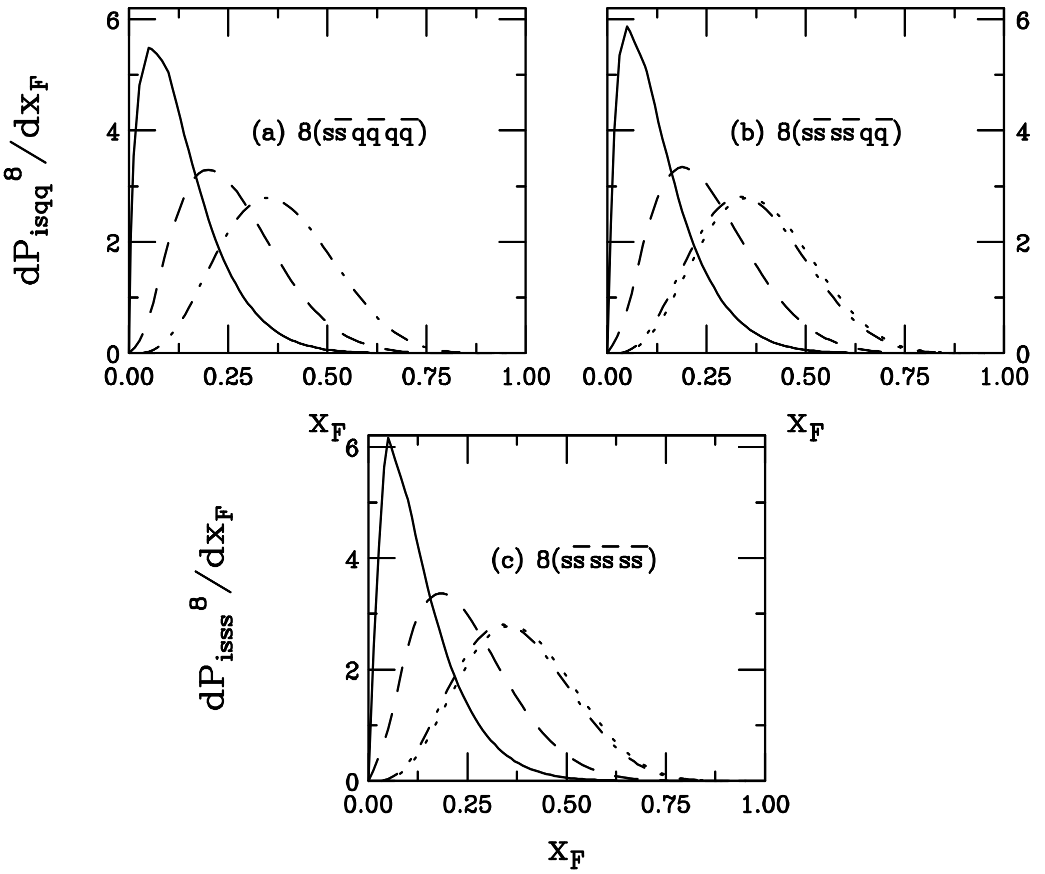

Figure 12: Strange hadron production in the intrinsic model from a π^- projectile in 8-particle Fock states with one, (a), two, (b), and three (c) $s\bar{s}$ pairs. The light quark pairs, denoted q, refer to both u and d quarks. Both the uncorrelated fragmentation and coalescence distributions are shown. The solid curve in each case is the strange quark distribution, also the hadron distribution from uncorrelated fragmentation. The other curves are the probability distributions for hadron production by coalescence. The dashed curves are the K meson distributions. The dot-dashed curves in (a) and (b) are baryons or antibaryons with a single $s/\bar{s}$ quark while the dot-dashed curve in (c) is the doubly-strange baryon/antibaryon distribution. The dotted curves in (b) is the doubly-strange baryon/antibaryon distributions while the dotted curve in (c) is the triply-strange $\Omega/\overline{\Omega}$ distribution.

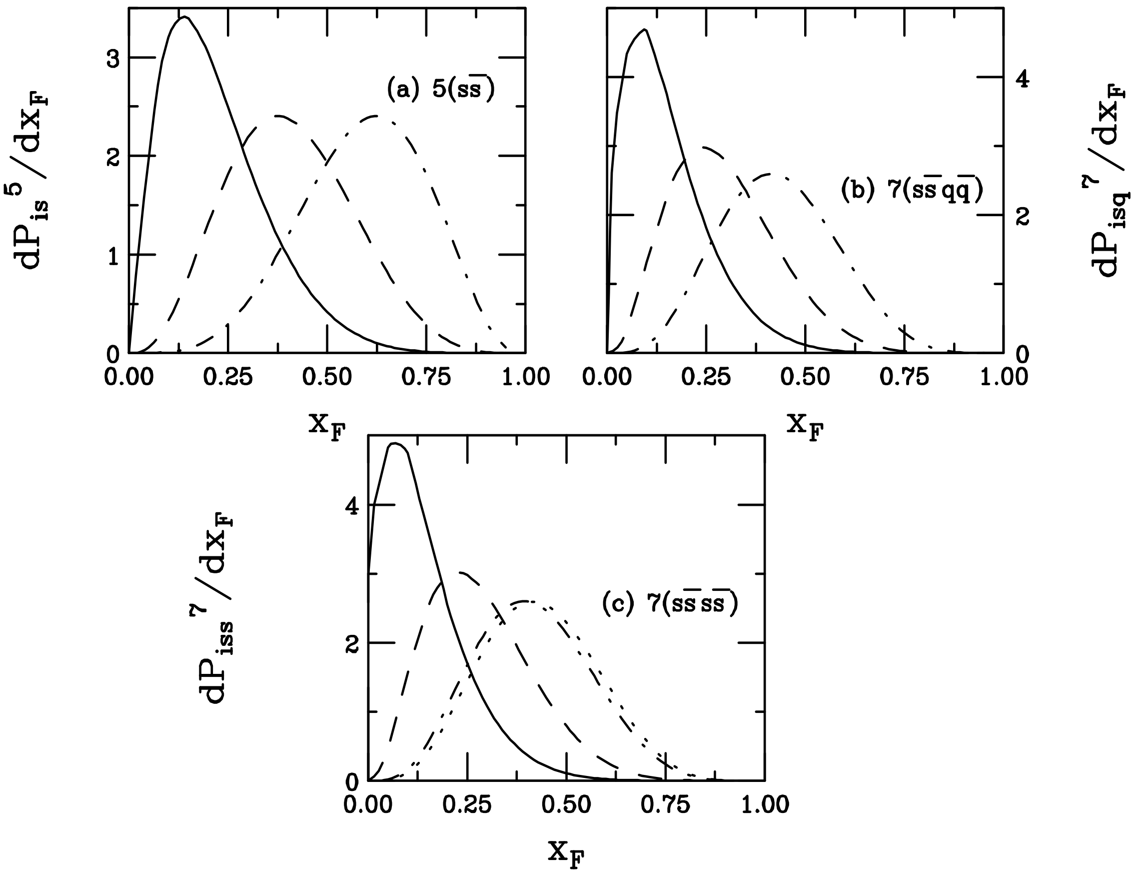

Figure 13: Strange hadron production in the intrinsic model from a proton projectile in a minimal 5-particle $s\overline{s}$ Fock state, (a), a 7-particle Fock state with one light quark pair, $q = u$ or d, and one $s\overline{s}$ pairs, (b), and with two $s\overline{s}$ pairs (c). Both the uncorrelated fragmentation and coalescence distributions are shown. The solid curve in each case is the strange quark distribution, also the hadron distribution from uncorrelated fragmentation. The other curves are the probability distributions for hadron production by coalescence. The dashed curves are the K meson distributions. The dot-dashed curves are baryons with a single strange quark, and the dotted curve in (c) is the doubly strange baryon distribution.

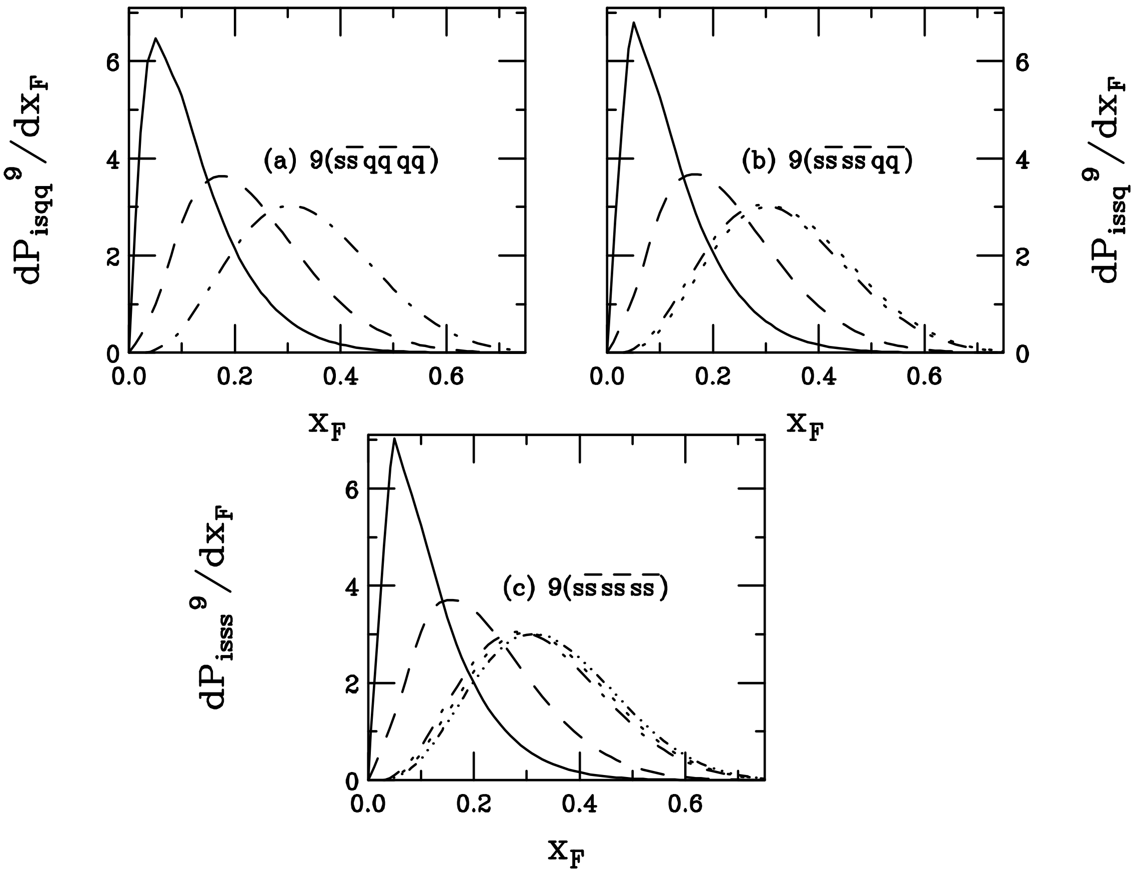

Figure 14: Strange hadron production in the intrinsic model from a proton projectile in 9-particle Fock states with one, (a), two, (b), and three (c) $s\overline{s}$ pairs. The light quark pairs, denoted q, refer to both u and d quarks. Both the uncorrelated fragmentation and coalescence distributions are shown. The solid curve in each case is the strange quark distribution, also the hadron distribution from uncorrelated fragmentation. The other curves are the probability distributions for hadron production by coalescence. The dashed curves are the K meson distributions. The dot-dashed curves are baryons or antibaryons (antibaryons in (a) only) with a single $s/\overline{s}$ quark, the dotted curves are doubly-strange baryons or antibaryons (antibaryons in (b) only), and the dot-dot-dot-dashed curve in (c) is the triply-strange $\Omega/\overline{\Omega}$.

It is clear from a comparison of the strange quark distributions in Figs. 13(a), 13(b), and 14(a) from five-, seven-, and nine-parton Fock states that the strange quark takes less of the projectile momentum as the number of partons in the configuration increases. These distributions correspond to production of all strange hadrons by uncorrelated fragmentation. As n increases, the strange quark distribution is suggestive of those in parameterizations of the parton distribution functions obtained from fits to data except for the behavior as $x_F \to 0$. If still more partons were included in the Fock state, the peak of the x_F distribution would occur at smaller x_F. The intrinsic model does not distinguish between "valence" and "sea" quarks in the state and treats all partons similarly except for the $\widehat{m}_Q^2$ weighting of each parton momentum fraction.

The coalescence curves are representative only since for example, in the dashed curve in Fig. 13(a), the only K mesons produced by coalescence from the $|uuds\overline{s}\rangle$ state are K^+ and K^0. The probability distributions are the same for both mesons before any weight factors are taken into account, as will be described later. These weights only change the relative normalization from a given state, not the shape of the distribution. In some of the higher Fock states, all K mesons can be produced by coalescence and then the meson probability distribution is the same for all kaons even though the weights are different for each meson. The same is true for the Λ and Σ^+ distributions in the dot-dashed curve in Fig. 13(a), and for all baryons with a single strange quark in the higher Fock states. When it is possible to produce baryons with more than one strange quark, the average x_F of the multiply-strange hadron is the largest of all the hadrons produced by coalescence because of the extra momentum imparted by the more massive strange quarks.

When eight- or nine-particle states are considered, both strange baryons and strange antibaryons can be produced by coalescence. In any given eight- or nine-particle Fock state then, the strange baryon and any antiparticle counterpart have the same probability distributions although they may have different weight factors. It is only the fact that, in most cases, the strange baryon can be produced in Fock states with fewer particles that gives it the "leading" edge over the strange antibaryon. This is especially true for the Ω and the $\overline{\Omega}$ which have equal probabilities and total intrinsic distributions from a pion but in a Σ^-, the Ω can already be produced by coalescence from a 7-particle Fock state while the $\overline{\Omega}$ is only produced by coalescence in the nine-particle $|ddss\overline{s}s\overline{s}s\overline{s}\rangle$ state.

The average momentum fractions, $\langle x_F\rangle$, of all these generic Fock states are given in Tables 4 and 5. The average momentum fractions carried by the strange quarks decreases $\sim 50\%$ for all projectile hadrons between the minimal and the nine-particle Fock states. On average the strange quarks carry more momentum in the pion because of its lower valence quark content. Also, in the four-parton Fock state, the K^- and K^0 can take half the pion momentum when produced by coalescence while the singly and doubly-strange baryons take half the pion momentum in the $|\overline{u}dq\overline{q}s\overline{s}\rangle$ and $|\overline{u}ds\overline{s}s\overline{s}\rangle$ six-parton Fock states respectively. In general, the strange baryons take more of the momentum from the lower p and Σ^- Fock states than from the pion while the strange mesons generally take less momentum from the proton than the pion. The situation is reversed between

State	Particle	$\langle x_F \rangle$	State	Particle	$\langle x_F \rangle$
$\vert\overline{u}d s\overline{s}\rangle$	s	0.272	$\vert\overline{u}d s\overline{s}q\overline{q}q\overline{q}\rangle$	s	0.138
"	$\overline{q}s = q\overline{s}$	0.500	"	$\overline{q}s = q\overline{s}$	0.258
$\vert\overline{u}d s\overline{s}q\overline{q}\rangle$	s	0.182	"	$qqs = \overline{qqs}$	0.379
"	$\overline{q}s = q\overline{s}$	0.342	$\vert\overline{u}d s\overline{s}s\overline{s}q\overline{q}\rangle$	s	0.133
"	$qqs = \overline{qqs}$	0.500	"	$\overline{q}s = q\overline{s}$	0.250
$\vert\overline{u}d s\overline{s}s\overline{s}\rangle$	s	0.173	"	$qqs = \overline{qqs}$	0.368
"	$\overline{q}s = q\overline{s}$	0.326	"	$qss = \overline{qss}$	0.382
"	$qss = \overline{qss}$	0.500	$\vert\overline{u}d s\overline{s}s\overline{s}s\overline{s}\rangle$	s	0.130
			"	$\overline{q}s = q\overline{s}$	0.243
			"	$qss = \overline{qss}$	0.371
			"	$sss = \overline{sss}$	0.384

Table 4: The average value of x_F for strange hadrons produced by fragmentation and coalescence from pion projectiles in 4, 6, and 8 parton configurations with $q = u$ or d.

the eight-parton states of the pion and the nine-parton states of the proton and Σ^- because the additional parton in the projectile baryons dilutes the available momentum for coalescence sufficiently to reduce the $\langle x_F \rangle$ with a baryon projectile relative to a pion projectile.

State	Particle	$\langle x_F \rangle$	State	Particle	$\langle x_F \rangle$
$\|uuds\overline{s}\rangle$	s	0.220	$\|uuds\overline{s}q\overline{q}q\overline{q}\rangle$	s	0.123
"	$\overline{q}s = q\overline{s}$	0.407	"	$\overline{q}s = q\overline{s}$	0.230
"	qqs	0.593	"	$qqs = \overline{qqs}$	0.338
$\|uuds\overline{s}q\overline{q}\rangle$	s	0.157	$\|uuds\overline{s}s\overline{s}q\overline{q}\rangle$	s	0.120
"	$\overline{q}s = q\overline{s}$	0.295	"	$\overline{q}s = q\overline{s}$	0.223
"	qqs	0.432	"	qqs	0.330
$\|uuds\overline{s}s\overline{s}\rangle$	s	0.150	"	$qss = \overline{qss}$	0.342
"	$\overline{q}s = q\overline{s}$	0.283	$\|uuds\overline{s}s\overline{s}s\overline{s}\rangle$	s	0.118
"	qqs	0.416	"	$\overline{q}s = q\overline{s}$	0.218
"	qss	0.434	"	qqs	0.323
			"	qss	0.333
			"	$sss = \overline{sss}$	0.344

Table 5: The average value of x_F for strange hadrons produced by fragmentation and coalescence from proton projectiles in 5, 7, and 9 parton configurations with $q = u$ or d.

Appendix B

Here we give the total probability distributions for strange and antistrange hadron production from the intrinsic model from π^- and p projectiles. Production from all states with up to three additional $Q\overline{Q}$ pairs in the Fock configuration is included. The probability distributions for each possible final state combination from uncorrelated fragmentation and coalescence are given in Figs. 11-14. We sum all the probabilities over the all the states for each projectile to find the total strange hadron x_F distribution from the intrinsic model. Thus, from Eq. (B.1), we have

$$\frac{dP_S}{dx_F} = \sum_n \sum_{r_u} \sum_{r_d} \sum_{r_s} \beta \left(\frac{1}{10} \frac{dP^{nF}_{\mathrm{i}(r_s\mathrm{s})(r_u\mathrm{u})(r_d\mathrm{d})}}{dx_F} + \xi \frac{dP^{nC}_{\mathrm{i}(r_s\mathrm{s})(r_u\mathrm{u})(r_d\mathrm{d})}}{dx_F} \right) \tag{B.1}$$

The weight of each state produced by coalescence is ξ where $\xi = 0$ when S cannot be produced by coalescence from state $|n_v r_s(s\overline{s}) r_u(u\overline{u}) r_d(d\overline{d})\rangle$. The parameter β is 1 when $\xi = 0$ and 0.5 when production by both fragmentation and coalescence is possible to conserve probability in each state. When we assume coalescence production only, $P^{nF} \equiv 0$ and $\beta \equiv 1$. The number of up, down and strange $Q\overline{Q}$ pairs is indicated by r_u, r_d and r_s respectively. The total, $r_u + r_d + r_s = r$, is defined as $r = (n - n_v)/2$ because each Q in an n-parton state is accompanied by a $\overline{Q}$. For baryon projectiles, $n = 5$, 7, and 9 while for mesons $n = 4$, 6, and 8. Depending on the value of n, r_i can be 0, 1, 2 or 3, *e.g.* in a $|uuds\overline{s}d\overline{d}d\overline{d}\rangle$ state, $r_u = 0$, $r_d = 2$ and $r_s = 1$ with $r = 3$. We note that the predictions for Λ and Σ^0 are identical because their quark content is the same. The normalized probabilities for the Fock states with two and three additional $Q\overline{Q}$ pairs are given in Eqs. (8)-(11). Recall that $P^5_{\mathrm{is}} = 0.02$.

The strange and antistrange hadron probability distributions from a π^- projectile are:

$$\begin{aligned}
\frac{dP_{K^+}}{dx_F} &= \frac{1}{10}\frac{dP^{4F}_{\rm is}}{dx_F} + \frac{1}{2}\left(\frac{1}{10}\frac{dP^{6F}_{\rm isu}}{dx_F} + \frac{1}{4}\frac{dP^{6C}_{\rm isu}}{dx_F}\right) + \frac{1}{10}\frac{dP^{6F}_{\rm isd}}{dx_F} + \frac{1}{10}\frac{dP^{6F}_{\rm iss}}{dx_F} \\
&+ \frac{1}{2}\left(\frac{1}{10}\frac{dP^{8F}_{\rm isuu}}{dx_F} + \frac{2}{7}\frac{dP^{8C}_{\rm isuu}}{dx_F}\right) + \frac{1}{2}\left(\frac{1}{10}\frac{dP^{8F}_{\rm isud}}{dx_F} + \frac{1}{7}\frac{dP^{8C}_{\rm isud}}{dx_F}\right) \\
&+ \frac{1}{10}\frac{dP^{8F}_{\rm isdd}}{dx_F} + \frac{1}{2}\left(\frac{1}{10}\frac{dP^{8F}_{\rm issu}}{dx_F} + \frac{2}{12}\frac{dP^{8C}_{\rm issu}}{dx_F}\right) + \frac{1}{10}\frac{dP^{8F}_{\rm issd}}{dx_F} + \frac{1}{10}\frac{dP^{8F}_{\rm isss}}{dx_F} \ , \qquad (B.2) \\
\frac{dP_{K^0}}{dx_F} &= \frac{1}{2}\left(\frac{1}{10}\frac{dP^{4F}_{\rm is}}{dx_F} + \frac{1}{2}\frac{dP^{4C}_{\rm is}}{dx_F}\right) + \frac{1}{2}\left(\frac{1}{10}\frac{dP^{6F}_{\rm isu}}{dx_F} + \frac{1}{4}\frac{dP^{6C}_{\rm isu}}{dx_F}\right) \\
&+ \frac{1}{2}\left(\frac{1}{10}\frac{dP^{6F}_{\rm isd}}{dx_F} + \frac{2}{4}\frac{dP^{6C}_{\rm isd}}{dx_F}\right) + \frac{1}{2}\left(\frac{1}{10}\frac{dP^{6F}_{\rm iss}}{dx_F} + \frac{2}{7}\frac{dP^{6C}_{\rm iss}}{dx_F}\right) \\
&+ \frac{1}{2}\left(\frac{1}{10}\frac{dP^{8F}_{\rm isuu}}{dx_F} + \frac{1}{7}\frac{dP^{8C}_{\rm isuu}}{dx_F}\right) + \frac{1}{2}\left(\frac{1}{10}\frac{dP^{8F}_{\rm isud}}{dx_F} + \frac{2}{7}\frac{dP^{8C}_{\rm isud}}{dx_F}\right) \\
&+ \frac{1}{2}\left(\frac{1}{10}\frac{dP^{8F}_{\rm isdd}}{dx_F} + \frac{3}{7}\frac{dP^{8C}_{\rm isdd}}{dx_F}\right) + \frac{1}{2}\left(\frac{1}{10}\frac{dP^{8F}_{\rm issu}}{dx_F} + \frac{2}{12}\frac{dP^{8C}_{\rm issu}}{dx_F}\right) \\
&+ \frac{1}{2}\left(\frac{1}{10}\frac{dP^{8F}_{\rm issd}}{dx_F} + \frac{4}{12}\frac{dP^{8C}_{\rm issd}}{dx_F}\right) + \frac{1}{2}\left(\frac{1}{10}\frac{dP^{8F}_{\rm isss}}{dx_F} + \frac{3}{16}\frac{dP^{8C}_{\rm isss}}{dx_F}\right) \ , \qquad (B.3) \\
\frac{dP_{K^-}}{dx_F} &= \frac{1}{2}\left(\frac{1}{10}\frac{dP^{4F}_{\rm is}}{dx_F} + \frac{1}{2}\frac{dP^{4C}_{\rm is}}{dx_F}\right) + \frac{1}{2}\left(\frac{1}{10}\frac{dP^{6F}_{\rm isu}}{dx_F} + \frac{2}{4}\frac{dP^{6C}_{\rm isu}}{dx_F}\right) \\
&+ \frac{1}{2}\left(\frac{1}{10}\frac{dP^{6F}_{\rm isd}}{dx_F} + \frac{1}{4}\frac{dP^{6C}_{\rm isd}}{dx_F}\right) + \frac{1}{2}\left(\frac{1}{10}\frac{dP^{6F}_{\rm iss}}{dx_F} + \frac{2}{7}\frac{dP^{6C}_{\rm iss}}{dx_F}\right) \\
&+ \frac{1}{2}\left(\frac{1}{10}\frac{dP^{8F}_{\rm isuu}}{dx_F} + \frac{3}{7}\frac{dP^{8C}_{\rm isuu}}{dx_F}\right) + \frac{1}{2}\left(\frac{1}{10}\frac{dP^{8F}_{\rm isud}}{dx_F} + \frac{2}{7}\frac{dP^{8C}_{\rm isud}}{dx_F}\right) \\
&+ \frac{1}{2}\left(\frac{1}{10}\frac{dP^{8F}_{\rm isdd}}{dx_F} + \frac{1}{7}\frac{dP^{8C}_{\rm isdd}}{dx_F}\right) + \frac{1}{2}\left(\frac{1}{10}\frac{dP^{8F}_{\rm issu}}{dx_F} + \frac{4}{12}\frac{dP^{8C}_{\rm issu}}{dx_F}\right) \\
&+ \frac{1}{2}\left(\frac{1}{10}\frac{dP^{8F}_{\rm issd}}{dx_F} + \frac{2}{12}\frac{dP^{8C}_{\rm issd}}{dx_F}\right) + \frac{1}{2}\left(\frac{1}{10}\frac{dP^{8F}_{\rm isss}}{dx_F} + \frac{3}{16}\frac{dP^{8C}_{\rm isss}}{dx_F}\right) \ , \qquad (B.4) \\
\frac{dP_{\overline{K}^0}}{dx_F} &= \frac{1}{10}\frac{dP^{4F}_{\rm is}}{dx_F} + \frac{1}{10}\frac{dP^{6F}_{\rm isu}}{dx_F} + \frac{1}{2}\left(\frac{1}{10}\frac{dP^{6F}_{\rm isd}}{dx_F} + \frac{1}{4}\frac{dP^{6C}_{\rm isd}}{dx_F}\right) + \frac{1}{10}\frac{dP^{6F}_{\rm iss}}{dx_F} \\
&+ \frac{1}{10}\frac{dP^{8F}_{\rm isuu}}{dx_F} + \frac{1}{2}\left(\frac{1}{10}\frac{dP^{8F}_{\rm isud}}{dx_F} + \frac{1}{7}\frac{dP^{8C}_{\rm isud}}{dx_F}\right) \\
&+ \frac{1}{2}\left(\frac{1}{10}\frac{dP^{8F}_{\rm isdd}}{dx_F} + \frac{2}{7}\frac{dP^{8C}_{\rm isdd}}{dx_F}\right) + \frac{1}{10}\frac{dP^{8F}_{\rm issu}}{dx_F} \\
&+ \frac{1}{2}\left(\frac{1}{10}\frac{dP^{8F}_{\rm issd}}{dx_F} + \frac{2}{12}\frac{dP^{8C}_{\rm issd}}{dx_F}\right) + \frac{1}{2}\left(\frac{1}{10}\frac{dP^{8F}_{\rm isss}}{dx_F} + \frac{3}{16}\frac{dP^{8C}_{\rm isss}}{dx_F}\right) \ , \qquad (B.5) \\
\frac{dP_{\Lambda}}{dx_F} &= \frac{dP_{\Sigma^0}}{dx_F} = \frac{1}{10}\frac{dP^{4F}_{\rm is}}{dx_F} + \frac{1}{2}\left(\frac{1}{10}\frac{dP^{6F}_{\rm isu}}{dx_F} + \frac{1}{4}\frac{dP^{6C}_{\rm isu}}{dx_F}\right) + \frac{1}{10}\frac{dP^{6F}_{\rm isd}}{dx_F} + \frac{1}{10}\frac{dP^{6F}_{\rm iss}}{dx_F}
\end{aligned}$$

$$
\begin{aligned}
&+\frac{1}{2}\left(\frac{1}{10}\frac{dP^{8F}_{\rm isuu}}{dx_F}+\frac{2}{7}\frac{dP^{8C}_{\rm isuu}}{dx_F}\right)+\frac{1}{2}\left(\frac{1}{10}\frac{dP^{8F}_{\rm isud}}{dx_F}+\frac{2}{7}\frac{dP^{8C}_{\rm isud}}{dx_F}\right)\\
&+\frac{1}{10}\frac{dP^{8F}_{\rm isdd}}{dx_F}+\frac{1}{2}\left(\frac{1}{10}\frac{dP^{8F}_{\rm issu}}{dx_F}+\frac{2}{12}\frac{dP^{8C}_{\rm issu}}{dx_F}\right)+\frac{1}{10}\frac{dP^{8F}_{\rm issd}}{dx_F}+\frac{1}{10}\frac{dP^{8F}_{\rm isss}}{dx_F}\ , \qquad \text{(B.6)}
\end{aligned}
$$

$$
\begin{aligned}
\frac{dP_{\Sigma^-}}{dx_F} &= \frac{1}{10}\frac{dP^{4F}_{\rm is}}{dx_F}+\frac{1}{10}\frac{dP^{6F}_{\rm isu}}{dx_F}+\frac{1}{2}\left(\frac{1}{10}\frac{dP^{6F}_{\rm isd}}{dx_F}+\frac{1}{4}\frac{dP^{6C}_{\rm isd}}{dx_F}\right)+\frac{1}{10}\frac{dP^{6F}_{\rm iss}}{dx_F}\\
&+\frac{1}{10}\frac{dP^{8F}_{\rm isuu}}{dx_F}+\frac{1}{2}\left(\frac{1}{10}\frac{dP^{8F}_{\rm isud}}{dx_F}+\frac{1}{7}\frac{dP^{8C}_{\rm isud}}{dx_F}\right)+\frac{1}{2}\left(\frac{1}{10}\frac{dP^{8F}_{\rm isdd}}{dx_F}+\frac{3}{7}\frac{dP^{8C}_{\rm isdd}}{dx_F}\right)\\
&+\frac{1}{10}\frac{dP^{8F}_{\rm issu}}{dx_F}+\frac{1}{2}\left(\frac{1}{10}\frac{dP^{8F}_{\rm issd}}{dx_F}+\frac{2}{12}\frac{dP^{8C}_{\rm issd}}{dx_F}\right)+\frac{1}{10}\frac{dP^{8F}_{\rm isss}}{dx_F}\ , \qquad \text{(B.7)}
\end{aligned}
$$

$$
\begin{aligned}
\frac{dP_{\Sigma^+}}{dx_F} &= \frac{1}{10}\frac{dP^{4F}_{\rm is}}{dx_F}+\frac{1}{10}\frac{dP^{6F}_{\rm isu}}{dx_F}+\frac{1}{10}\frac{dP^{6F}_{\rm isd}}{dx_F}+\frac{1}{10}\frac{dP^{6F}_{\rm iss}}{dx_F}+\frac{1}{2}\left(\frac{1}{10}\frac{dP^{8F}_{\rm isuu}}{dx_F}+\frac{1}{7}\frac{dP^{8C}_{\rm isuu}}{dx_F}\right)\\
&+\frac{1}{10}\frac{dP^{8F}_{\rm isud}}{dx_F}+\frac{1}{10}\frac{dP^{8F}_{\rm isdd}}{dx_F}+\frac{1}{10}\frac{dP^{8F}_{\rm issu}}{dx_F}+\frac{1}{10}\frac{dP^{8F}_{\rm issd}}{dx_F}+\frac{1}{10}\frac{dP^{8F}_{\rm isss}}{dx_F}\ , \qquad \text{(B.8)}
\end{aligned}
$$

$$
\begin{aligned}
\frac{dP_{\Xi^0}}{dx_F} &= \frac{1}{10}\frac{dP^{4F}_{\rm is}}{dx_F}+\frac{1}{10}\frac{dP^{6F}_{\rm isu}}{dx_F}+\frac{1}{10}\frac{dP^{6F}_{\rm isd}}{dx_F}+\frac{1}{10}\frac{dP^{6F}_{\rm iss}}{dx_F}+\frac{1}{10}\frac{dP^{8F}_{\rm isuu}}{dx_F}+\frac{1}{10}\frac{dP^{8F}_{\rm isud}}{dx_F}\\
&+\frac{1}{10}\frac{dP^{8F}_{\rm isdd}}{dx_F}+\frac{1}{2}\left(\frac{1}{10}\frac{dP^{8F}_{\rm issu}}{dx_F}+\frac{1}{12}\frac{dP^{8C}_{\rm issu}}{dx_F}\right)+\frac{1}{10}\frac{dP^{8F}_{\rm issd}}{dx_F}+\frac{1}{10}\frac{dP^{8F}_{\rm isss}}{dx_F}\ , \qquad \text{(B.9)}
\end{aligned}
$$

$$
\begin{aligned}
\frac{dP_{\Xi^-}}{dx_F} &= \frac{1}{10}\frac{dP^{4F}_{\rm is}}{dx_F}+\frac{1}{10}\frac{dP^{6F}_{\rm isu}}{dx_F}+\frac{1}{10}\frac{dP^{6F}_{\rm isd}}{dx_F}+\frac{1}{2}\left(\frac{1}{10}\frac{dP^{6F}_{\rm iss}}{dx_F}+\frac{1}{7}\frac{dP^{6C}_{\rm iss}}{dx_F}\right)\\
&+\frac{1}{10}\frac{dP^{8F}_{\rm isuu}}{dx_F}+\frac{1}{10}\frac{dP^{8F}_{\rm isud}}{dx_F}+\frac{1}{10}\frac{dP^{8F}_{\rm isdd}}{dx_F}+\frac{1}{2}\left(\frac{1}{10}\frac{dP^{8F}_{\rm issu}}{dx_F}+\frac{1}{12}\frac{dP^{8C}_{\rm issu}}{dx_F}\right)\\
&+\frac{1}{2}\left(\frac{1}{10}\frac{dP^{8F}_{\rm issd}}{dx_F}+\frac{2}{12}\frac{dP^{8C}_{\rm issd}}{dx_F}\right)+\frac{1}{2}\left(\frac{1}{10}\frac{dP^{8F}_{\rm isss}}{dx_F}+\frac{3}{16}\frac{dP^{8C}_{\rm isss}}{dx_F}\right)\ , \qquad \text{(B.10)}
\end{aligned}
$$

$$
\begin{aligned}
\frac{dP_{\Omega}}{dx_F} &= \frac{1}{10}\frac{dP^{4F}_{\rm is}}{dx_F}+\frac{1}{10}\frac{dP^{6F}_{\rm isu}}{dx_F}+\frac{1}{10}\frac{dP^{6F}_{\rm isd}}{dx_F}+\frac{1}{10}\frac{dP^{6F}_{\rm iss}}{dx_F}+\frac{1}{10}\frac{dP^{8F}_{\rm isuu}}{dx_F}+\frac{1}{10}\frac{dP^{8F}_{\rm isud}}{dx_F}\\
&+\frac{1}{10}\frac{dP^{8F}_{\rm isdd}}{dx_F}+\frac{1}{10}\frac{dP^{8F}_{\rm issu}}{dx_F}+\frac{1}{10}\frac{dP^{8F}_{\rm issd}}{dx_F}+\frac{1}{2}\left(\frac{1}{10}\frac{dP^{8F}_{\rm isss}}{dx_F}+\frac{1}{16}\frac{dP^{8C}_{\rm isss}}{dx_F}\right)\ , \qquad \text{(B.11)}
\end{aligned}
$$

$$
\begin{aligned}
\frac{dP_{\overline{\Lambda}}}{dx_F} &= \frac{dP_{\overline{\Sigma}^0}}{dx_F}=\frac{1}{10}\frac{dP^{4F}_{\rm is}}{dx_F}+\frac{1}{10}\frac{dP^{6F}_{\rm isu}}{dx_F}+\frac{1}{2}\left(\frac{1}{10}\frac{dP^{6F}_{\rm isd}}{dx_F}+\frac{1}{4}\frac{dP^{6C}_{\rm isd}}{dx_F}\right)+\frac{1}{10}\frac{dP^{6F}_{\rm iss}}{dx_F}\\
&+\frac{1}{10}\frac{dP^{8F}_{\rm isuu}}{dx_F}+\frac{1}{2}\left(\frac{1}{10}\frac{dP^{8F}_{\rm isud}}{dx_F}+\frac{2}{7}\frac{dP^{8C}_{\rm isud}}{dx_F}\right)+\frac{1}{2}\left(\frac{1}{10}\frac{dP^{8F}_{\rm isdd}}{dx_F}+\frac{2}{7}\frac{dP^{8C}_{\rm isdd}}{dx_F}\right)\\
&+\frac{1}{10}\frac{dP^{8F}_{\rm issu}}{dx_F}+\frac{1}{2}\left(\frac{1}{10}\frac{dP^{8F}_{\rm issd}}{dx_F}+\frac{2}{12}\frac{dP^{8C}_{\rm issd}}{dx_F}\right)+\frac{1}{10}\frac{dP^{8F}_{\rm isss}}{dx_F}\ , \qquad \text{(B.12)}
\end{aligned}
$$

$$
\begin{aligned}
\frac{dP_{\overline{\Sigma}^-}}{dx_F} &= \frac{1}{10}\frac{dP^{4F}_{\rm is}}{dx_F}+\frac{1}{10}\frac{dP^{6F}_{\rm isu}}{dx_F}+\frac{1}{10}\frac{dP^{6F}_{\rm isd}}{dx_F}+\frac{1}{10}\frac{dP^{6F}_{\rm iss}}{dx_F}+\frac{1}{10}\frac{dP^{8F}_{\rm isuu}}{dx_F}+\frac{1}{10}\frac{dP^{8F}_{\rm isud}}{dx_F}\\
&+\frac{1}{2}\left(\frac{1}{10}\frac{dP^{8F}_{\rm isdd}}{dx_F}+\frac{1}{7}\frac{dP^{8C}_{\rm isdd}}{dx_F}\right)+\frac{1}{10}\frac{dP^{8F}_{\rm issu}}{dx_F}+\frac{1}{10}\frac{dP^{8F}_{\rm issd}}{dx_F}+\frac{1}{10}\frac{dP^{8F}_{\rm isss}}{dx_F}\ , \qquad \text{(B.13)}
\end{aligned}
$$

$$
\begin{aligned}
\frac{dP_{\overline{\Sigma}^+}}{dx_F} &= \frac{1}{10}\frac{dP^{4F}_{\rm is}}{dx_F} + \frac{1}{2}\left(\frac{1}{10}\frac{dP^{6F}_{\rm isu}}{dx_F} + \frac{1}{4}\frac{dP^{6C}_{\rm isu}}{dx_F}\right) + \frac{1}{10}\frac{dP^{6F}_{\rm isd}}{dx_F} + \frac{1}{10}\frac{dP^{6F}_{\rm iss}}{dx_F} \\
&+ \frac{1}{2}\left(\frac{1}{10}\frac{dP^{8F}_{\rm isuu}}{dx_F} + \frac{3}{7}\frac{dP^{8C}_{\rm isuu}}{dx_F}\right) + \frac{1}{2}\left(\frac{1}{10}\frac{dP^{8F}_{\rm isud}}{dx_F} + \frac{1}{7}\frac{dP^{8C}_{\rm isud}}{dx_F}\right) \\
&+ \frac{1}{10}\frac{dP^{8F}_{\rm isdd}}{dx_F} + \frac{1}{2}\left(\frac{1}{10}\frac{dP^{8F}_{\rm issu}}{dx_F} + \frac{2}{12}\frac{dP^{8C}_{\rm issu}}{dx_F}\right) + \frac{1}{10}\frac{dP^{8F}_{\rm issd}}{dx_F} + \frac{1}{10}\frac{dP^{8F}_{\rm isss}}{dx_F} \ , \qquad \text{(B.14)} \\
\frac{dP_{\overline{\Xi}^0}}{dx_F} &= \frac{1}{10}\frac{dP^{4F}_{\rm is}}{dx_F} + \frac{1}{10}\frac{dP^{6F}_{\rm isu}}{dx_F} + \frac{1}{10}\frac{dP^{6F}_{\rm isd}}{dx_F} + \frac{1}{2}\left(\frac{1}{10}\frac{dP^{6F}_{\rm iss}}{dx_F} + \frac{1}{7}\frac{dP^{6C}_{\rm iss}}{dx_F}\right) \\
&+ \frac{1}{10}\frac{dP^{8F}_{\rm isuu}}{dx_F} + \frac{1}{10}\frac{dP^{8F}_{\rm isud}}{dx_F} + \frac{1}{10}\frac{dP^{8F}_{\rm isdd}}{dx_F} + \frac{1}{2}\left(\frac{1}{10}\frac{dP^{8F}_{\rm issu}}{dx_F} + \frac{2}{12}\frac{dP^{8C}_{\rm issu}}{dx_F}\right) \\
&+ \frac{1}{2}\left(\frac{1}{10}\frac{dP^{8F}_{\rm issd}}{dx_F} + \frac{1}{12}\frac{dP^{8C}_{\rm issd}}{dx_F}\right) + \frac{1}{2}\left(\frac{1}{10}\frac{dP^{8F}_{\rm isss}}{dx_F} + \frac{3}{16}\frac{dP^{8C}_{\rm isss}}{dx_F}\right) \ , \qquad \text{(B.15)} \\
\frac{dP_{\overline{\Xi}^-}}{dx_F} &= \frac{1}{10}\frac{dP^{4F}_{\rm is}}{dx_F} + \frac{1}{10}\frac{dP^{6F}_{\rm isu}}{dx_F} + \frac{1}{10}\frac{dP^{6F}_{\rm isd}}{dx_F} + \frac{1}{10}\frac{dP^{6F}_{\rm iss}}{dx_F} + \frac{1}{10}\frac{dP^{8F}_{\rm isuu}}{dx_F} + \frac{1}{10}\frac{dP^{8F}_{\rm isud}}{dx_F} \\
&+ \frac{1}{10}\frac{dP^{8F}_{\rm isdd}}{dx_F} + \frac{1}{10}\frac{dP^{8F}_{\rm issu}}{dx_F} + \frac{1}{2}\left(\frac{1}{10}\frac{dP^{8F}_{\rm issd}}{dx_F} + \frac{1}{12}\frac{dP^{8C}_{\rm issd}}{dx_F}\right) + \frac{1}{10}\frac{dP^{8F}_{\rm isss}}{dx_F} \ , \qquad \text{(B.16)} \\
\frac{dP_{\overline{\Omega}}}{dx_F} &= \frac{1}{10}\frac{dP^{4F}_{\rm is}}{dx_F} + \frac{1}{10}\frac{dP^{6F}_{\rm isu}}{dx_F} + \frac{1}{10}\frac{dP^{6F}_{\rm isd}}{dx_F} + \frac{1}{10}\frac{dP^{6F}_{\rm iss}}{dx_F} + \frac{1}{10}\frac{dP^{8F}_{\rm isuu}}{dx_F} + \frac{1}{10}\frac{dP^{8F}_{\rm isud}}{dx_F} \\
&+ \frac{1}{10}\frac{dP^{8F}_{\rm isdd}}{dx_F} + \frac{1}{10}\frac{dP^{8F}_{\rm issu}}{dx_F} + \frac{1}{10}\frac{dP^{8F}_{\rm issd}}{dx_F} + \frac{1}{2}\left(\frac{1}{10}\frac{dP^{8F}_{\rm isss}}{dx_F} + \frac{1}{16}\frac{dP^{8C}_{\rm isss}}{dx_F}\right) \ . \qquad \text{(B.17)}
\end{aligned}
$$

The strange and antistrange hadron probability distributions from a proton projectile are:

$$
\begin{aligned}
\frac{dP_{K^+}}{dx_F} &= \frac{1}{2}\left(\frac{1}{10}\frac{dP^{5F}_{\rm is}}{dx_F} + \frac{2}{4}\frac{dP^{5C}_{\rm is}}{dx_F}\right) + \frac{1}{2}\left(\frac{1}{10}\frac{dP^{7F}_{\rm isu}}{dx_F} + \frac{3}{5}\frac{dP^{7C}_{\rm isu}}{dx_F}\right) \\
&+ \frac{1}{2}\left(\frac{1}{10}\frac{dP^{7F}_{\rm isd}}{dx_F} + \frac{2}{5}\frac{dP^{7C}_{\rm isd}}{dx_F}\right) + \frac{1}{2}\left(\frac{1}{10}\frac{dP^{7F}_{\rm iss}}{dx_F} + \frac{4}{10}\frac{dP^{7C}_{\rm iss}}{dx_F}\right) \\
&+ \frac{1}{2}\left(\frac{1}{10}\frac{dP^{9F}_{\rm isuu}}{dx_F} + \frac{4}{7}\frac{dP^{9C}_{\rm isuu}}{dx_F}\right) + \frac{1}{2}\left(\frac{1}{10}\frac{dP^{9F}_{\rm isud}}{dx_F} + \frac{3}{7}\frac{dP^{9C}_{\rm isud}}{dx_F}\right) \\
&+ \frac{1}{2}\left(\frac{1}{10}\frac{dP^{9F}_{\rm isdd}}{dx_F} + \frac{2}{7}\frac{dP^{9C}_{\rm isdd}}{dx_F}\right) + \frac{1}{2}\left(\frac{1}{10}\frac{dP^{9F}_{\rm issu}}{dx_F} + \frac{6}{13}\frac{dP^{9C}_{\rm issu}}{dx_F}\right) \\
&+ \frac{1}{2}\left(\frac{1}{10}\frac{dP^{9F}_{\rm issd}}{dx_F} + \frac{4}{13}\frac{dP^{9C}_{\rm issd}}{dx_F}\right) + \frac{1}{2}\left(\frac{1}{10}\frac{dP^{9F}_{\rm isss}}{dx_F} + \frac{6}{19}\frac{dP^{9C}_{\rm isss}}{dx_F}\right) \ , \qquad \text{(B.18)} \\
\frac{dP_{K^0}}{dx_F} &= \frac{1}{2}\left(\frac{1}{10}\frac{dP^{5F}_{\rm is}}{dx_F} + \frac{1}{4}\frac{dP^{5C}_{\rm is}}{dx_F}\right) + \frac{1}{2}\left(\frac{1}{10}\frac{dP^{7F}_{\rm isu}}{dx_F} + \frac{1}{5}\frac{dP^{7C}_{\rm isu}}{dx_F}\right) \\
&+ \frac{1}{2}\left(\frac{1}{10}\frac{dP^{7F}_{\rm isd}}{dx_F} + \frac{2}{5}\frac{dP^{7C}_{\rm isd}}{dx_F}\right) + \frac{1}{2}\left(\frac{1}{10}\frac{dP^{7F}_{\rm iss}}{dx_F} + \frac{2}{10}\frac{dP^{7C}_{\rm iss}}{dx_F}\right) \\
&+ \frac{1}{2}\left(\frac{1}{10}\frac{dP^{9F}_{\rm isuu}}{dx_F} + \frac{1}{7}\frac{dP^{9C}_{\rm isuu}}{dx_F}\right) + \frac{1}{2}\left(\frac{1}{10}\frac{dP^{9F}_{\rm isud}}{dx_F} + \frac{2}{7}\frac{dP^{9C}_{\rm isud}}{dx_F}\right)
\end{aligned}
$$

$$
\begin{aligned}
&+\frac{1}{2}\left(\frac{1}{10}\frac{dP^{9F}_{\rm isdd}}{dx_F}+\frac{3}{7}\frac{dP^{9C}_{\rm isdd}}{dx_F}\right)+\frac{1}{2}\left(\frac{1}{10}\frac{dP^{9F}_{\rm issu}}{dx_F}+\frac{2}{13}\frac{dP^{9C}_{\rm issu}}{dx_F}\right)\\
&+\frac{1}{2}\left(\frac{1}{10}\frac{dP^{9F}_{\rm issd}}{dx_F}+\frac{4}{13}\frac{dP^{9C}_{\rm issd}}{dx_F}\right)+\frac{1}{2}\left(\frac{1}{10}\frac{dP^{9F}_{\rm isss}}{dx_F}+\frac{3}{19}\frac{dP^{9C}_{\rm isss}}{dx_F}\right)\ , \qquad \text{(B.19)}
\end{aligned}
$$

$$
\begin{aligned}
\frac{dP_{K^-}}{dx_F} =& \frac{1}{10}\frac{dP^{5F}_{\rm is}}{dx_F}+\frac{1}{2}\left(\frac{1}{10}\frac{dP^{7F}_{\rm isu}}{dx_F}+\frac{1}{8}\frac{dP^{7C}_{\rm isu}}{dx_F}\right)+\frac{1}{10}\frac{dP^{7F}_{\rm isd}}{dx_F}+\frac{1}{10}\frac{dP^{7F}_{\rm iss}}{dx_F}\\
&+\frac{1}{2}\left(\frac{1}{10}\frac{dP^{9F}_{\rm isuu}}{dx_F}+\frac{2}{13}\frac{dP^{9C}_{\rm isuu}}{dx_F}\right)+\frac{1}{2}\left(\frac{1}{10}\frac{dP^{9F}_{\rm isud}}{dx_F}+\frac{1}{13}\frac{dP^{9C}_{\rm isud}}{dx_F}\right)\\
&+\frac{1}{10}\frac{dP^{9F}_{\rm isdd}}{dx_F}+\frac{1}{2}\left(\frac{1}{10}\frac{dP^{9F}_{\rm issu}}{dx_F}+\frac{2}{22}\frac{dP^{9C}_{\rm issu}}{dx_F}\right)+\frac{1}{10}\frac{dP^{9F}_{\rm issd}}{dx_F}+\frac{1}{10}\frac{dP^{9F}_{\rm isss}}{dx_F}\ , \qquad \text{(B.20)}
\end{aligned}
$$

$$
\begin{aligned}
\frac{dP_{\overline{K}^0}}{dx_F} =& \frac{1}{10}\frac{dP^{5F}_{\rm is}}{dx_F}+\frac{1}{10}\frac{dP^{7F}_{\rm isu}}{dx_F}+\frac{1}{2}\left(\frac{1}{10}\frac{dP^{7F}_{\rm isd}}{dx_F}+\frac{1}{8}\frac{dP^{7C}_{\rm isd}}{dx_F}\right)+\frac{1}{10}\frac{dP^{7F}_{\rm iss}}{dx_F}\\
&+\frac{1}{10}\frac{dP^{9F}_{\rm isuu}}{dx_F}+\frac{1}{2}\left(\frac{1}{10}\frac{dP^{9F}_{\rm isud}}{dx_F}+\frac{1}{13}\frac{dP^{9C}_{\rm isud}}{dx_F}\right)+\frac{1}{2}\left(\frac{1}{10}\frac{dP^{9F}_{\rm isdd}}{dx_F}+\frac{2}{13}\frac{dP^{9C}_{\rm isdd}}{dx_F}\right)\\
&+\frac{1}{10}\frac{dP^{9F}_{\rm issu}}{dx_F}+\frac{1}{2}\left(\frac{1}{10}\frac{dP^{9F}_{\rm issd}}{dx_F}+\frac{2}{22}\frac{dP^{9C}_{\rm issd}}{dx_F}\right)+\frac{1}{10}\frac{dP^{9F}_{\rm isss}}{dx_F}\ , \qquad \text{(B.21)}
\end{aligned}
$$

$$
\begin{aligned}
\frac{dP_{\Lambda}}{dx_F} =& \frac{dP_{\Sigma^0}}{dx_F}=\frac{1}{2}\left(\frac{1}{10}\frac{dP^{5F}_{\rm is}}{dx_F}+\frac{2}{4}\frac{dP^{5C}_{\rm is}}{dx_F}\right)+\frac{1}{2}\left(\frac{1}{10}\frac{dP^{7F}_{\rm isu}}{dx_F}+\frac{3}{8}\frac{dP^{7C}_{\rm isu}}{dx_F}\right)\\
&+\frac{1}{2}\left(\frac{1}{10}\frac{dP^{7F}_{\rm isd}}{dx_F}+\frac{4}{8}\frac{dP^{7C}_{\rm isd}}{dx_F}\right)+\frac{1}{2}\left(\frac{1}{10}\frac{dP^{7F}_{\rm iss}}{dx_F}+\frac{4}{13}\frac{dP^{7C}_{\rm iss}}{dx_F}\right)\\
&+\frac{1}{2}\left(\frac{1}{10}\frac{dP^{9F}_{\rm isuu}}{dx_F}+\frac{4}{13}\frac{dP^{9C}_{\rm isuu}}{dx_F}\right)+\frac{1}{2}\left(\frac{1}{10}\frac{dP^{9F}_{\rm isud}}{dx_F}+\frac{6}{13}\frac{dP^{9C}_{\rm isud}}{dx_F}\right)\\
&+\frac{1}{2}\left(\frac{1}{10}\frac{dP^{9F}_{\rm isdd}}{dx_F}+\frac{6}{13}\frac{dP^{9C}_{\rm isdd}}{dx_F}\right)+\frac{1}{2}\left(\frac{1}{10}\frac{dP^{9F}_{\rm issu}}{dx_F}+\frac{6}{22}\frac{dP^{9C}_{\rm issu}}{dx_F}\right)\\
&+\frac{1}{2}\left(\frac{1}{10}\frac{dP^{9F}_{\rm issd}}{dx_F}+\frac{8}{22}\frac{dP^{9C}_{\rm issd}}{dx_F}\right)+\frac{1}{2}\left(\frac{1}{10}\frac{dP^{9F}_{\rm isss}}{dx_F}+\frac{6}{22}\frac{dP^{9C}_{\rm isss}}{dx_F}\right)\ , \qquad \text{(B.22)}
\end{aligned}
$$

$$
\begin{aligned}
\frac{dP_{\Sigma^-}}{dx_F} =& \frac{1}{10}\frac{dP^{5F}_{\rm is}}{dx_F}+\frac{1}{10}\frac{dP^{7F}_{\rm isu}}{dx_F}+\frac{1}{2}\left(\frac{1}{10}\frac{dP^{7F}_{\rm isd}}{dx_F}+\frac{1}{8}\frac{dP^{7C}_{\rm isd}}{dx_F}\right)+\frac{1}{10}\frac{dP^{7F}_{\rm iss}}{dx_F}\\
&+\frac{1}{10}\frac{dP^{9F}_{\rm isuu}}{dx_F}+\frac{1}{2}\left(\frac{1}{10}\frac{dP^{9F}_{\rm isud}}{dx_F}+\frac{1}{13}\frac{dP^{9C}_{\rm isud}}{dx_F}\right)+\frac{1}{2}\left(\frac{1}{10}\frac{dP^{9F}_{\rm isdd}}{dx_F}+\frac{3}{13}\frac{dP^{9C}_{\rm isdd}}{dx_F}\right)\\
&+\frac{1}{10}\frac{dP^{9F}_{\rm issu}}{dx_F}+\frac{1}{2}\left(\frac{1}{10}\frac{dP^{9F}_{\rm issd}}{dx_F}+\frac{2}{22}\frac{dP^{9C}_{\rm issd}}{dx_F}\right)+\frac{1}{10}\frac{dP^{9F}_{\rm isss}}{dx_F}\ , \qquad \text{(B.23)}
\end{aligned}
$$

$$
\begin{aligned}
\frac{dP_{\Sigma^+}}{dx_F} =& \frac{1}{2}\left(\frac{1}{10}\frac{dP^{5F}_{\rm is}}{dx_F}+\frac{1}{4}\frac{dP^{5C}_{\rm is}}{dx_F}\right)+\frac{1}{2}\left(\frac{1}{10}\frac{dP^{7F}_{\rm isu}}{dx_F}+\frac{3}{8}\frac{dP^{7C}_{\rm isu}}{dx_F}\right)\\
&+\frac{1}{2}\left(\frac{1}{10}\frac{dP^{7F}_{\rm isd}}{dx_F}+\frac{1}{8}\frac{dP^{7C}_{\rm isd}}{dx_F}\right)+\frac{1}{2}\left(\frac{1}{10}\frac{dP^{7F}_{\rm iss}}{dx_F}+\frac{2}{13}\frac{dP^{7C}_{\rm iss}}{dx_F}\right)\\
&+\frac{1}{2}\left(\frac{1}{10}\frac{dP^{9F}_{\rm isuu}}{dx_F}+\frac{6}{13}\frac{dP^{9C}_{\rm isuu}}{dx_F}\right)+\frac{1}{2}\left(\frac{1}{10}\frac{dP^{9F}_{\rm isud}}{dx_F}+\frac{3}{13}\frac{dP^{9C}_{\rm isud}}{dx_F}\right)
\end{aligned}
$$

$$
\begin{aligned}
&+\frac{1}{2}\left(\frac{1}{10}\frac{dP^{9F}_{\rm isdd}}{dx_F}+\frac{1}{13}\frac{dP^{9C}_{\rm isdd}}{dx_F}\right)+\frac{1}{2}\left(\frac{1}{10}\frac{dP^{9F}_{\rm issu}}{dx_F}+\frac{6}{22}\frac{dP^{9C}_{\rm issu}}{dx_F}\right)\\
&+\frac{1}{2}\left(\frac{1}{10}\frac{dP^{9F}_{\rm issd}}{dx_F}+\frac{2}{22}\frac{dP^{9C}_{\rm issd}}{dx_F}\right)+\frac{1}{2}\left(\frac{1}{10}\frac{dP^{9F}_{\rm isss}}{dx_F}+\frac{3}{28}\frac{dP^{9C}_{\rm isss}}{dx_F}\right)\ , \qquad \text{(B.24)}
\end{aligned}
$$

$$
\begin{aligned}
\frac{dP_{\Xi^0}}{dx_F} = {}& \frac{1}{10}\frac{dP^{5F}_{\rm is}}{dx_F}+\frac{1}{10}\frac{dP^{7F}_{\rm isu}}{dx_F}+\frac{1}{10}\frac{dP^{7F}_{\rm isd}}{dx_F}+\frac{1}{2}\left(\frac{1}{10}\frac{dP^{7F}_{\rm iss}}{dx_F}+\frac{2}{13}\frac{dP^{7C}_{\rm iss}}{dx_F}\right)\\
&+\frac{1}{10}\frac{dP^{9F}_{\rm isuu}}{dx_F}+\frac{1}{10}\frac{dP^{9F}_{\rm isud}}{dx_F}+\frac{1}{10}\frac{dP^{9F}_{\rm isdd}}{dx_F}+\frac{1}{2}\left(\frac{1}{10}\frac{dP^{9F}_{\rm issu}}{dx_F}+\frac{3}{22}\frac{dP^{9C}_{\rm issu}}{dx_F}\right)\\
&+\frac{1}{2}\left(\frac{1}{10}\frac{dP^{9F}_{\rm issd}}{dx_F}+\frac{2}{22}\frac{dP^{9C}_{\rm issd}}{dx_F}\right)+\frac{1}{2}\left(\frac{1}{10}\frac{dP^{9F}_{\rm isss}}{dx_F}+\frac{6}{28}\frac{dP^{9C}_{\rm isss}}{dx_F}\right)\ , \qquad \text{(B.25)}
\end{aligned}
$$

$$
\begin{aligned}
\frac{dP_{\Xi^-}}{dx_F} = {}& \frac{1}{10}\frac{dP^{5F}_{\rm is}}{dx_F}+\frac{1}{10}\frac{dP^{7F}_{\rm isu}}{dx_F}+\frac{1}{10}\frac{dP^{7F}_{\rm isd}}{dx_F}+\frac{1}{2}\left(\frac{1}{10}\frac{dP^{7F}_{\rm iss}}{dx_F}+\frac{1}{13}\frac{dP^{7C}_{\rm iss}}{dx_F}\right)\\
&+\frac{1}{10}\frac{dP^{9F}_{\rm isuu}}{dx_F}+\frac{1}{10}\frac{dP^{9F}_{\rm isud}}{dx_F}+\frac{1}{10}\frac{dP^{9F}_{\rm isdd}}{dx_F}+\frac{1}{2}\left(\frac{1}{10}\frac{dP^{9F}_{\rm issu}}{dx_F}+\frac{1}{22}\frac{dP^{9C}_{\rm issu}}{dx_F}\right)\\
&+\frac{1}{2}\left(\frac{1}{10}\frac{dP^{9F}_{\rm issd}}{dx_F}+\frac{2}{22}\frac{dP^{9C}_{\rm issd}}{dx_F}\right)+\frac{1}{2}\left(\frac{1}{10}\frac{dP^{9F}_{\rm isss}}{dx_F}+\frac{3}{28}\frac{dP^{9C}_{\rm isss}}{dx_F}\right)\ , \qquad \text{(B.26)}
\end{aligned}
$$

$$
\begin{aligned}
\frac{dP_{\Omega}}{dx_F} = {}& \frac{1}{10}\frac{dP^{5F}_{\rm is}}{dx_F}+\frac{1}{10}\frac{dP^{7F}_{\rm isu}}{dx_F}+\frac{1}{10}\frac{dP^{7F}_{\rm isd}}{dx_F}+\frac{1}{10}\frac{dP^{7F}_{\rm iss}}{dx_F}+\frac{1}{10}\frac{dP^{9F}_{\rm isuu}}{dx_F}+\frac{1}{10}\frac{dP^{9F}_{\rm isud}}{dx_F}\\
&+\frac{1}{10}\frac{dP^{9F}_{\rm isdd}}{dx_F}+\frac{1}{10}\frac{dP^{9F}_{\rm issu}}{dx_F}+\frac{1}{10}\frac{dP^{9F}_{\rm issd}}{dx_F}+\frac{1}{2}\left(\frac{1}{10}\frac{dP^{9F}_{\rm isss}}{dx_F}+\frac{1}{28}\frac{dP^{9C}_{\rm isss}}{dx_F}\right)\ , \qquad \text{(B.27)}
\end{aligned}
$$

$$
\begin{aligned}
\frac{dP_{\overline{\Lambda}}}{dx_F} = {}& \frac{dP_{\overline{\Sigma}^0}}{dx_F}=\frac{1}{10}\frac{dP^{5F}_{\rm is}}{dx_F}+\frac{1}{10}\frac{dP^{7F}_{\rm isu}}{dx_F}+\frac{1}{10}\frac{dP^{7F}_{\rm isd}}{dx_F}+\frac{1}{10}\frac{dP^{7F}_{\rm iss}}{dx_F}\\
&+\frac{1}{10}\frac{dP^{9F}_{\rm isuu}}{dx_F}+\frac{1}{2}\left(\frac{1}{10}\frac{dP^{9F}_{\rm isud}}{dx_F}+\frac{1}{7}\frac{dP^{9C}_{\rm isud}}{dx_F}\right)+\frac{1}{10}\frac{dP^{9F}_{\rm isdd}}{dx_F}+\frac{1}{10}\frac{dP^{9F}_{\rm issu}}{dx_F}\\
&+\frac{1}{10}\frac{dP^{9F}_{\rm issd}}{dx_F}+\frac{1}{10}\frac{dP^{9F}_{\rm isss}}{dx_F}\ , \qquad \text{(B.28)}
\end{aligned}
$$

$$
\begin{aligned}
\frac{dP_{\overline{\Sigma}^-}}{dx_F} = {}& \frac{1}{10}\frac{dP^{5F}_{\rm is}}{dx_F}+\frac{1}{10}\frac{dP^{7F}_{\rm isu}}{dx_F}+\frac{1}{10}\frac{dP^{7F}_{\rm isd}}{dx_F}+\frac{1}{10}\frac{dP^{7F}_{\rm iss}}{dx_F}+\frac{1}{10}\frac{dP^{9F}_{\rm isuu}}{dx_F}+\frac{1}{10}\frac{dP^{9F}_{\rm isud}}{dx_F}\\
&+\frac{1}{2}\left(\frac{1}{10}\frac{dP^{9F}_{\rm isdd}}{dx_F}+\frac{1}{7}\frac{dP^{9C}_{\rm isdd}}{dx_F}\right)+\frac{1}{10}\frac{dP^{9F}_{\rm issu}}{dx_F}+\frac{1}{10}\frac{dP^{9F}_{\rm issd}}{dx_F}+\frac{1}{10}\frac{dP^{9F}_{\rm isss}}{dx_F}\ , \qquad \text{(B.29)}
\end{aligned}
$$

$$
\begin{aligned}
\frac{dP_{\overline{\Sigma}^+}}{dx_F} = {}& \frac{1}{10}\frac{dP^{5F}_{\rm is}}{dx_F}+\frac{1}{10}\frac{dP^{7F}_{\rm isu}}{dx_F}+\frac{1}{10}\frac{dP^{7F}_{\rm isd}}{dx_F}+\frac{1}{10}\frac{dP^{7F}_{\rm iss}}{dx_F}+\frac{1}{2}\left(\frac{1}{10}\frac{dP^{9F}_{\rm isuu}}{dx_F}+\frac{1}{7}\frac{dP^{9C}_{\rm isuu}}{dx_F}\right)\\
&+\frac{1}{10}\frac{dP^{9F}_{\rm isud}}{dx_F}+\frac{1}{10}\frac{dP^{9F}_{\rm isdd}}{dx_F}+\frac{1}{10}\frac{dP^{9F}_{\rm issu}}{dx_F}+\frac{1}{10}\frac{dP^{9F}_{\rm issd}}{dx_F}+\frac{1}{10}\frac{dP^{9F}_{\rm isss}}{dx_F}\ , \qquad \text{(B.30)}
\end{aligned}
$$

$$
\begin{aligned}
\frac{dP_{\overline{\Xi}^0}}{dx_F} = {}& \frac{1}{10}\frac{dP^{5F}_{\rm is}}{dx_F}+\frac{1}{10}\frac{dP^{7F}_{\rm isu}}{dx_F}+\frac{1}{10}\frac{dP^{7F}_{\rm isd}}{dx_F}+\frac{1}{10}\frac{dP^{7F}_{\rm iss}}{dx_F}+\frac{1}{10}\frac{dP^{9F}_{\rm isuu}}{dx_F}+\frac{1}{10}\frac{dP^{9F}_{\rm isud}}{dx_F}\\
&+\frac{1}{10}\frac{dP^{9F}_{\rm isdd}}{dx_F}+\frac{1}{2}\left(\frac{1}{10}\frac{dP^{9F}_{\rm issu}}{dx_F}+\frac{1}{13}\frac{dP^{9C}_{\rm issu}}{dx_F}\right)+\frac{1}{10}\frac{dP^{9F}_{\rm issd}}{dx_F}+\frac{1}{10}\frac{dP^{9F}_{\rm isss}}{dx_F}\ , \qquad \text{(B.31)}
\end{aligned}
$$

$$\frac{dP_{\overline{\Xi}^-}}{dx_F} = \frac{1}{10}\frac{dP^{5F}_{\mathrm{is}}}{dx_F} + \frac{1}{10}\frac{dP^{7F}_{\mathrm{isu}}}{dx_F} + \frac{1}{10}\frac{dP^{7F}_{\mathrm{isd}}}{dx_F} + \frac{1}{10}\frac{dP^{7F}_{\mathrm{iss}}}{dx_F} + \frac{1}{10}\frac{dP^{9F}_{\mathrm{isuu}}}{dx_F} + \frac{1}{10}\frac{dP^{9F}_{\mathrm{isud}}}{dx_F}$$
$$+ \frac{1}{10}\frac{dP^{9F}_{\mathrm{isdd}}}{dx_F} + \frac{1}{10}\frac{dP^{9F}_{\mathrm{issu}}}{dx_F} + \frac{1}{2}\left(\frac{1}{10}\frac{dP^{9F}_{\mathrm{issd}}}{dx_F} + \frac{1}{13}\frac{dP^{9C}_{\mathrm{issd}}}{dx_F}\right) + \frac{1}{10}\frac{dP^{9F}_{\mathrm{isss}}}{dx_F}\ , \tag{B.32}$$

$$\frac{dP_{\overline{\Omega}}}{dx_F} = \frac{1}{10}\frac{dP^{5F}_{\mathrm{is}}}{dx_F} + \frac{1}{10}\frac{dP^{7F}_{\mathrm{isu}}}{dx_F} + \frac{1}{10}\frac{dP^{7F}_{\mathrm{isd}}}{dx_F} + \frac{1}{10}\frac{dP^{7F}_{\mathrm{iss}}}{dx_F} + \frac{1}{10}\frac{dP^{9F}_{\mathrm{isuu}}}{dx_F} + \frac{1}{10}\frac{dP^{9F}_{\mathrm{isud}}}{dx_F}$$
$$+ \frac{1}{10}\frac{dP^{9F}_{\mathrm{isdd}}}{dx_F} + \frac{1}{10}\frac{dP^{9F}_{\mathrm{issu}}}{dx_F} + \frac{1}{10}\frac{dP^{9F}_{\mathrm{issd}}}{dx_F} + \frac{1}{2}\left(\frac{1}{10}\frac{dP^{9F}_{\mathrm{isss}}}{dx_F} + \frac{1}{19}\frac{dP^{9C}_{\mathrm{isss}}}{dx_F}\right)\ . \tag{B.33}$$